Study of Fast Patrol Boat Models with and Without Tunnels on The Effect of Resistance Using Computational Fluid Dynamics

Microplastic Characteristic Found in Gastrointestinal Tract Of Pelagic and Demersal Fishes in Tuban, East Java

Designing A Boat Hotel (Botel) for Marine Tourism on Tabuhan Island, Banyuwangi Regency, East Java

Integration Analysis of Drone Multi Sensor-GNSS-Lidar-Camera For 3d Mapping (Case Study: PT Garam, Pamekasan, Madura)

Identification of Groundwater Potential Using Geographic Information Systems and Remote Sensing (Case Study: Mojokerto Regency)

https://journal.its.ac.id/index.php/jmest

Editor's Note :

In the fast-growing of science and technology in marine-earth related topics, we would like to launch a new international journal entitled Marine-Earth Science and Technology Journal (JMEST). The new journal isaimed as a media communication amongst scientists and engineers in thefields of marine and earth science and technology and will receive re- search and technical papers to be reviewed by our editors and reviewers.The JMEST will be issued three times a year and the first issue consist of 5 (five) papers from Malaysia and Indonesia.

Scopes of Journal :

Marine Science, Naval Architecture, Ship Production Technology, Marine Engineering, Marine Technology, Marine Transportation and Logistics, Ocean Renewable Energy, Earth Science, Physical Oceanography, Ocean and Atmospheric Interaction, Geology and Marine Geology, Geothermal Engineering, Geophysics, Disaster Management and Mitigation, Coastal Environmental Protection.

Table Of Contents

STUDY OF FAST PATROL BOAT MODELS WITH AND WITHOUT TUNNELS ON THE EFFECT OF RESISTANCE USING COMPUTATIONAL FLUID DYNAMICS

Sutiyo[1], Ali Munazid[1], Gde A. Prabhawatya Poundra[1], Bagiyo Swasono[2]

[1]Department of Naval Architecture, Universitas Hang Tuah, Surabaya, Indonesia
[2]Department of Ocean Engineering, Universitas Hang Tuah, Surabaya, Indonesia

E-mail: sutiyo@hangtuah.ac.id

ABSTRACT

Archipelagic countries need modern ships for maritime security, so it is necessary to create effective fast patrol boats. This research is focused on designs with and without a tunnel at the bottom to determine the design with the least resistance. CFD offers accurate findings to compare the problems faced by two different types of fast patrol boats. Calculation of the use without tunnels, the use of tunnels on fast patrol boats reduces the average drag of 5.4%. According to the CFD simulation results, the use of tunnels can greatly reduce the high pressure at the bottom in interaction with the water flow. Utilization of using tunnels is a solution that can be used more successfully for fast patrol boat operations.

Keyword: Fast Patrol Boat, CFD, Resistance, With Tunnel, Without Tunnel

Introduction

Convention on the Law of the Sea (UNCLOS) of 1982 recognized Indonesia as an archipelagic nation [1]. Indonesia is comprised of 17,504 islands, of which two-thirds are water/seas. As the world's biggest archipelago with the fourth-longest coastline, Indonesia boasts an abundance of marine resources. However, these resources cannot be efficiently managed to promote the welfare of the populace. Even the protection of the maritime ecosystem has not received sufficient consideration.

The Indonesian seas are experiencing a decline in quality due to rampant activities that have a negative impact on sea conditions, such as illegal fishing, destruction of coral reefs and environmental pollution [2]. This is a challenge for the Indonesian nation in the future, how can this enormous wealth be utilized for the greatest possible benefit of society in a sustainable manner. Like other developing countries in the world, Indonesia is also still facing problems in managing, conserving and protecting marine areas and their ecosystems and natural resources [3].

The defence and security of Indonesia are heavily impacted by global and regional strategic factors. Indonesia is the only archipelagic state to have identified archipelagic sea lanes in connection with the determination of the rite of passage through archipelagic sea lanes. There are three north-to-south and reverse archipelagic sea lanes that cross through Indonesia.

The Indonesian Archipelagic Sea Lanes (ALKI) can be used for global and regional purposes. With this access, it makes the territory of Indonesia vulnerable to attacks [4]. There are many different kinds of threats in the maritime world, and most of the time, each country or party decides what kind of threat it is based on the threat itself and how vulnerable the party that feels threatened is. Some people think that disputes between countries, maritime terrorism, piracy, narcotics smuggling, people smuggling, weapons enrichment or proliferation, illegal fishing, pollution, maritime accidents, and natural disasters are all threats in the maritime field. With this threat, the law enforcement agencies that are in charge of keeping the Indonesian seas safe need to take action.

For this reason, Indonesia needs competent fast patrol boats.

The efficiency and effectiveness of a ship's operations are greatly enhanced by its hull's design [5]. In addition, the use of tunnels on the bottom of fast patrol boats also affects operational performance [6]. The distribution of pressure around the tunnel area changes with tunnel area ratio, and all three design conditions studied showed a consistent reduction in resistance [7]. The usage of tunnel at high-speed planning vessels have aero-hydrodynamic qualities to decrease drag, good sea-keeping behaviour, reduce slamming, and prevent purposing [8],[9]. A new parameter called tunnel efficiency has been introduced. The tunnel efficiency is the range of speeds where a planning hull's tunnel is most effective at reducing drag [10].

This research was conducted with the aim of knowing and studying the performance of fast patrol boats in bottom variations, with and without tunnels. A computational fluid dynamics approach is used in this study to determine the effect of bottom variations on fast patrol boats on resistance. Simulation and data verification are carried out according to ITTC regulations.

Methodology

Numerical Governing Equation

Computational Fluid Dynamics (CFD) technique was used to predict the resistance of models. Utama [11] have carried out research on calculating the hull resistance of slender catamaran by using CFD, and showed good results compared to experiments. The Reynolds-averaged Navier-Stokes (RANS) method is a three-dimensional equation developed and used in the CFD model. The flow problems in the walls of ship are solved using unsteady incompressible flow such as provided by ANSYS-CFX [12].

In the modeling of wake fields, it is discovered that the selection of turbulence models is very important. This study makes use of the SST (Shear Stress Transport) turbulence model created by Menter [13][14]. The SST model has been utilized and verified by many researchers, all of whom have had positive findings using the model [15][16][17]. The RANS solver, which is implemented in ANSYS CFX, is used to solve the fluid flow field. Equations (1), (2), and (3) describe the continuity, RANS, and SST turbulence equations, respectively, as follow:

Continuity equation:

$$\frac{\partial \rho}{\partial t} + \frac{\partial}{\partial x_j}\left(\rho U_j\right) = 0 \tag{1}$$

The continuity equation was defined that ρ is fluid density, *t* is time, U_j is the flow velocity vector field.

RANS equation:

$$\rho \bar{f}_i + \frac{\partial}{\partial x_j}\left[-\bar{p}\delta_{ij} + \mu\left(\frac{\partial \bar{u}_i}{\partial x_j} + \frac{\partial \bar{u}_j}{\partial x_i}\right) - \overline{\rho u_i' u_j'}\right] - \rho \bar{u}_j \frac{\partial \bar{u}_i}{\partial x_j} = 0 \tag{2}$$

The left side of RANS equation represents the change in mean momentum of fluid element to the unsteadiness in the mean flow. This change is balanced by the mean body force ($\bar{f}$), the mean pressure field ($\bar{p}$), the viscous stress, $\mu\left(\frac{\partial \bar{u}_i}{\partial x_j} + \frac{\partial \bar{u}_j}{\partial x_i}\right)$, and apparent stress ($\rho u_i' u_j'$) to the fluctuating velocity field.

Menter's SST equation

$$\frac{\gamma}{v_t} P - \beta \rho \omega^2 + \frac{\partial}{\partial x_i}\left[(\mu + \sigma_\omega \mu_t)\frac{\partial \omega}{\partial x_i}\right] + 2(1 - F_1)2\rho_{\omega 2}\frac{1}{\omega}\frac{\partial k}{\partial x_i}\frac{\partial \omega}{\partial x_i} - \left(\frac{\partial(\rho\omega)}{\partial t} + \frac{\partial(\rho u_j \omega)}{\partial x_i}\right) = 0 \tag{3}$$

The Menter's SST model combines the advantages of the k-ω model to achieve an optimal model formulation for a wide range of applications. For this, a blending function F1 is introduced which is equal to one near the solid surface and equal to zero for the flow domain away from the wall. It activates the k-ω wall region and the k-ε model for residual flow. By this approach, the attractive near-wall performance of the k-ω model can be used for the free stream sensitivity.

Geometry Model

As shown in Figure 1, the hull geometry of fast patrol boat with no axe-bow, semi axe-bow and axe-bow modification. The main dimensions of the models are listed in Table 1.
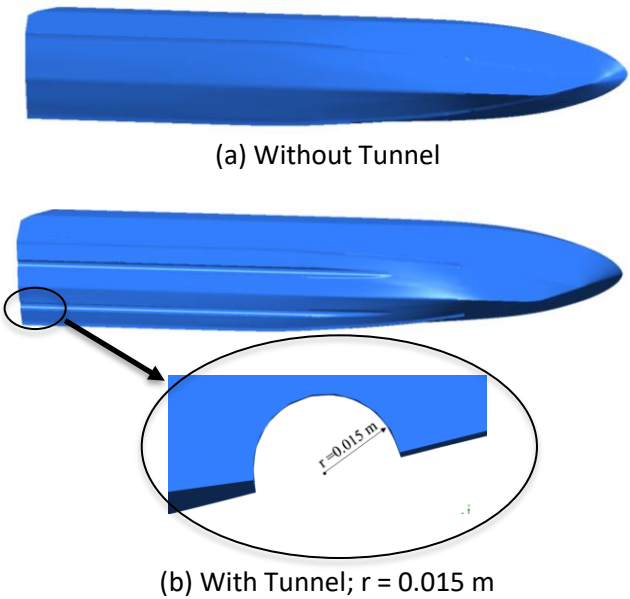

(a) Without Tunnel

(b) With Tunnel; r = 0.015 m

Figure 1. Fast Patrol Boat Model

Table 1. Main dimension of fast patrol boat models

Dimension	Unit	With Tunnel	Without tunnel
Length Over All (L_{OA})	m	2	2
Length Water Line (L_{WL})	m	1.823	1.823
Breadth (B)	m	0.356	0.356
Heigh (H)	m	0.265	0.265
Draft (T)	m	0.692	0.690
Wetted Surface Area (S)	m^2	0.628	0.566
Displacement (Δ)	kg	20.98	20.98
Coefficient Block (C_B)		0.529	0.532

Boundary Condition

The proposed computational domain is 2L forward, perpendicular to the front, at the velocity inlet, and 5L towards the rear, perpendicular to the outlet pressure. By adjusting the transverse and vertical directions to 2L-3L [30], we were able to prevent the negative impact of reverse flow on the borders of the area. Both the domain size and the boundary conditions are shown in Figure 5. Inlet flow velocity is defined as Fr = 0.3 to 0.8, and outlet hydrostatic pressure is defined as a function of water level; the hull body is identified as a fixed boundary and a no-slip condition; the bottom is given a free-slip condition; the top wall is given an opening condition; and the side walls are given a symmetry condition, as shown at Figure 2.
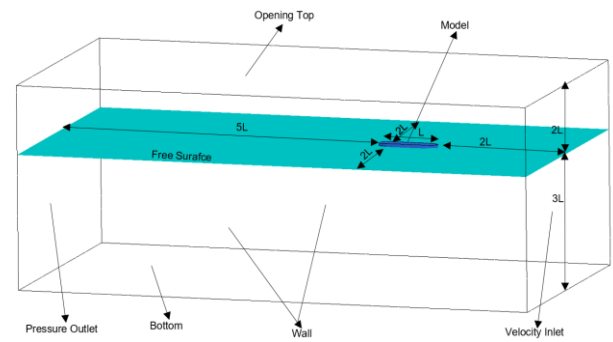
Figure 2. Boundary Condition Setting

Meshing and Grid Independence Study

The use of Design Modeler was required to complete the process of mesh construction for this investigation. A combination of structured and unstructured meshes are used in order to discretize the computation domain. In consideration of the intricate geometrical features of the hull, a mesh consisting of triangle elements is constructed on the surface of the hull. Subsequently, the boundary layer is refined using prism elements that are generated by expanding the surface mesh node. Inflated tetrahedral elements are used to populate the area close to the boat, while an unstructured mesh with grid generation is used to reduce the total number of components in the distant field (as illustrated in Figure 3).
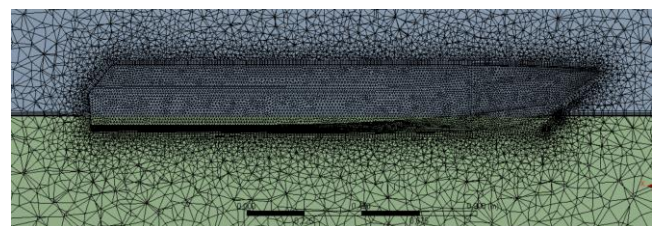
(a) Side view
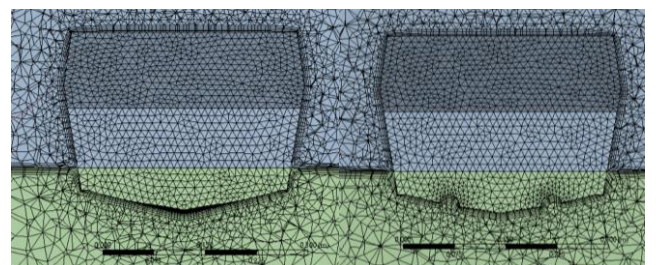
(b) Without tunnel mid-section	(c) With tunnel mid-section

A fine mesh may always deliver reliable results in ANSYS CFX, but at the same time, it increases the computational cost and time consumption owing to the huge element number. The mesh size plays a significant part in the calculation operation. Mesh convergence experiments are performed on both the fast patrol boat model with a tunnel and one without

a tunnel at a Froude number of 0.4. This is done so that the mesh size may be determined with an acceptable level of numerical accuracy and the total number of elements, as shown in Figure 4, which presents the results of the grid independence study. The number of elements used in the fast patrol boat model with a tunnel was approximately 1.9 million, while the number of elements used in the fast patrol boat model without a tunnel was approximately 1.7 million.

Result and Discussion

Figure 5 illustrates the computation used to determine the resistance of the two models. Although the difference is not statistically significant, the fact that it exists has a beneficial impact on the process of tunnel construction on rapid patrol boats. As can be seen in Figure 5, the resistance differential is at its lowest with a value of 3.2% when Fr is equal to 0.3, while it is at its greatest value when Fr is equal to 0.8 with a value of 7.2%.

Figure 4. Grid Independence Study
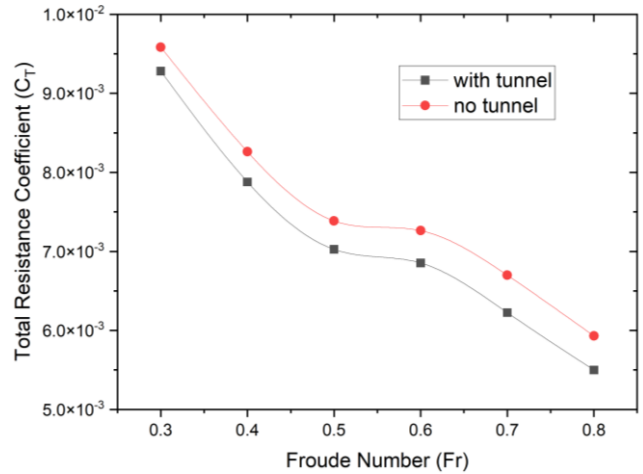
Figure 5. The differences CT at Fast Patrol Boat Models
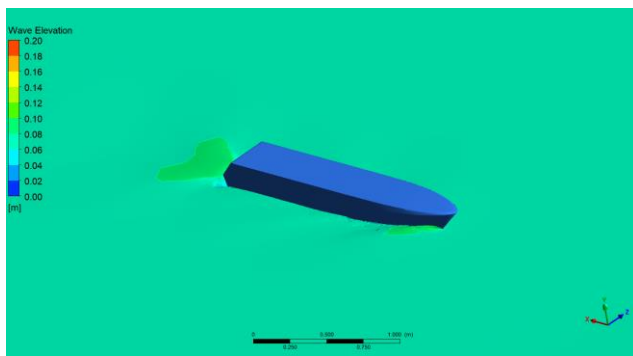
(i) with without tunnel
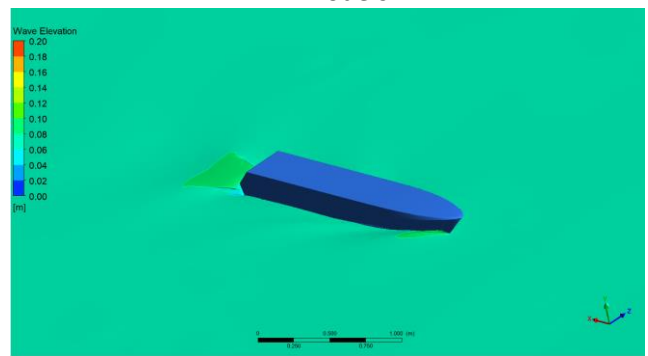
(ii) with tunnel

(a) Wave generation

(i) with without tunnel

(ii) with tunnel

(b) Pressure distribution at bottom

Figure 6. Wave elevation and Pressure distribution of Fast Patrol Model at High Speed (Fr=0.8)

Figure 7. Lateral pressure distribution at 0.1L from stern of bottom at Fr = 0.3

An interesting appearance emerges while comparing the two different models of fast patrol boats, one of which has tunnels and the other of which does not. Both of these models were analysed, one with a low speed of Fr = 0.3, one with a medium speed of Fr = 0.5, and one with a high speed of Fr. 0.8. This study was performed on the difference in pressure on the bottom of the ship as a result of the use of tunnels and their influence on resistance. Tunnels are an effect of the use of tunnels. This phenomenon is clearly illustrated as shown in Figure 6-11.

Figure 6.ai demonstrates wave forming on the two models' fronts. The model scale height of 0.09 m makes little effect. This occurrence does not explain the two models' resistance differences. The details are there for the taking, the model without a tunnel (Figure 6.a.i) has a pooled flow that increases the hull pull, while the model with a tunnel (Figure 6.a.ii) has a more pointed flow pattern that reduces the drag of the fluid against the model ship's hull.

The bottom pressure of the two swift patrol boat variants increases as resistance decreases. Figures 6.b and 7 show that the rapid patrol boat model with tunnels has a pressure distribution value of 3.25% higher than the one without tunnels. Figure 11 shows that the tunnel pressure dropped 5.34%, corroborating the considerable drag reduction reported. The tunnel on this quick patrol boat reduces drag by 3.2% at Fr 0.3.

(i) with without tunnel   (ii) with tunnel
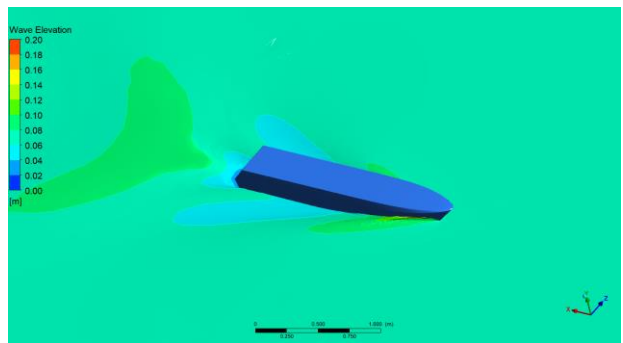
(a) Wave generation
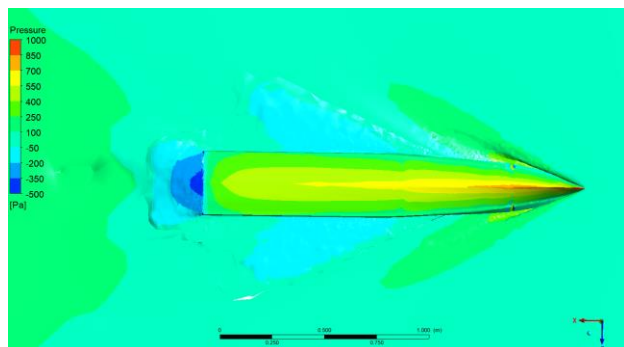
(i) with without tunnel   (ii) with tunnel
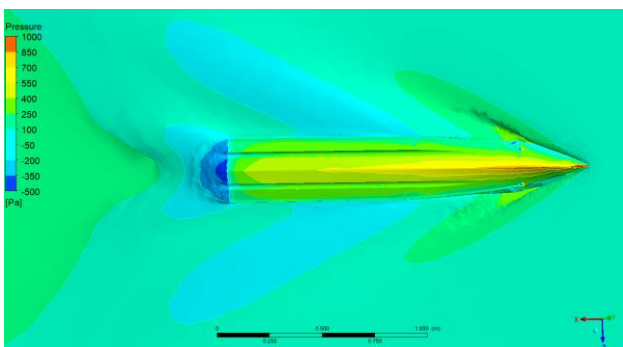
(b) Pressure distribution at bottom

Figure 8. Wave elevation and Pressure distribution of Fast Patrol Model at High Speed (Fr=0.5)

without a tunnel exhibiting a pooled flow that causes the hull pull to be greater, and the model with a tunnel exhibiting a more pointed flow pattern that shows a more directed fluid flow and provides a reduced drag of the fluid against the hull of the model ship.

Both types of fast patrol boats experience a rise in pressure underneath their hulls as a result of a decrease in resistance. Figures 8.b and 9 show that the pressure distribution trends of the fast patrol boat model with and without tunnels are similar, but that the pressure distribution value is different by around 3.27% between the two models. Figure 11 displays the average percentage drop in tunnel pressure, which at 6.51% lends credence to the significant reduction in drag reported. As an added bonus, at a speed of 0.5 Fr, the tunnel installed on this fast patrol boat reduces total drag by 4.68%.

Figure 9. Lateral pressure distribution at 0.1L from stern of bottom at Fr = 0.5

The drag reduction is quite significant at Fr=0.8 as mentioned in Figure 5. Figure 10 (a.i) shows the occurrence of wave making on the front side of the two models. In general, there is no significant difference with a height of about 0.13 m at the model scale.

Wave generation of side front hull is seen in Figure 8.a for both models. With a height of around 0.05 m at the model scale, there is no discernible change in the usual case. The discrepancy in resistance between the two models is not due to this occurrence. However, if you look closely, you can see that the flow pattern behind the model is quite different, with the model
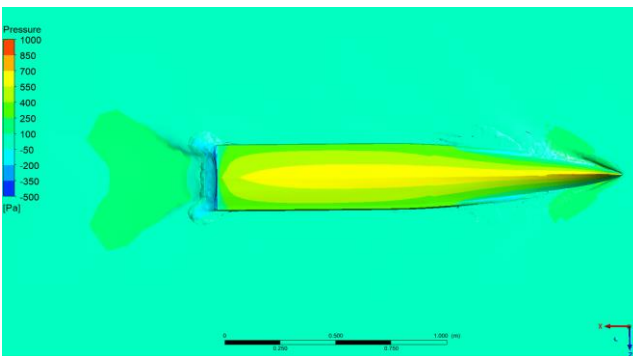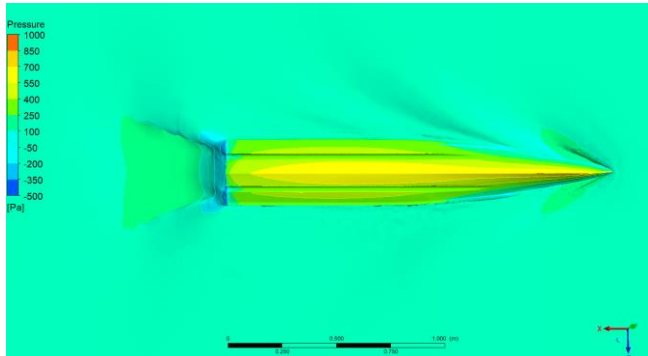

(i) with without tunnel	(ii) with tunnel

(a) Wave generation
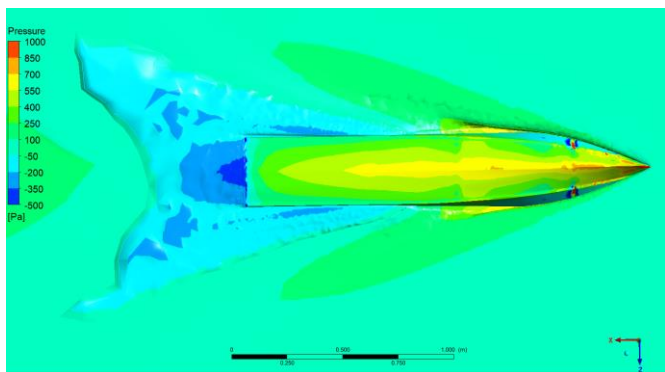
(i) with without tunnel	(ii) with tunnel
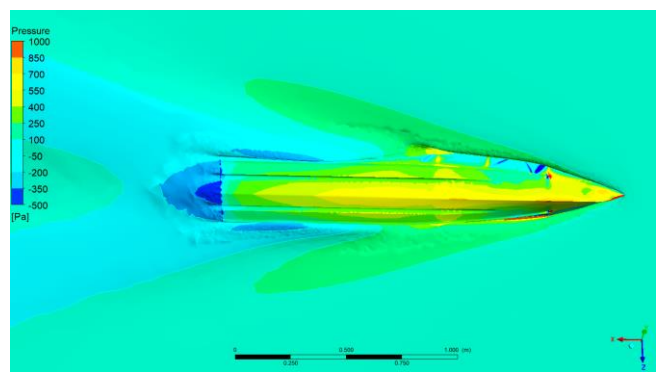
(b) Pressure distribution at bottom

Figure 10. Wave elevation and Pressure distribution of Fast Patrol Model at High Speed (Fr=0.8)
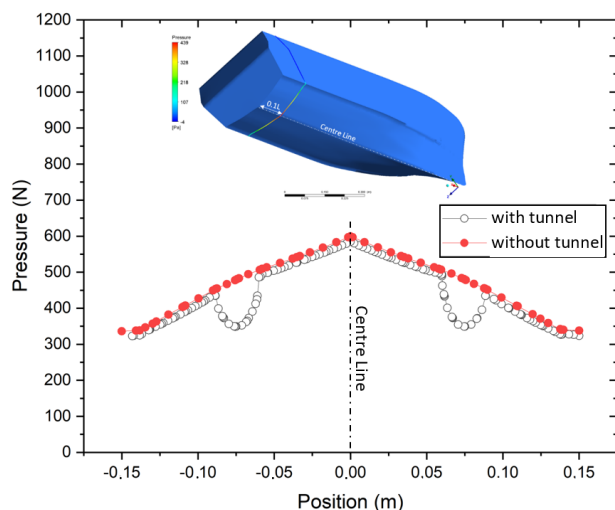
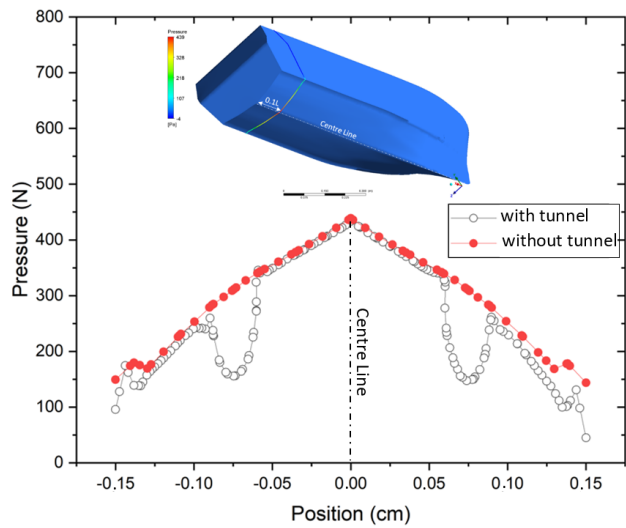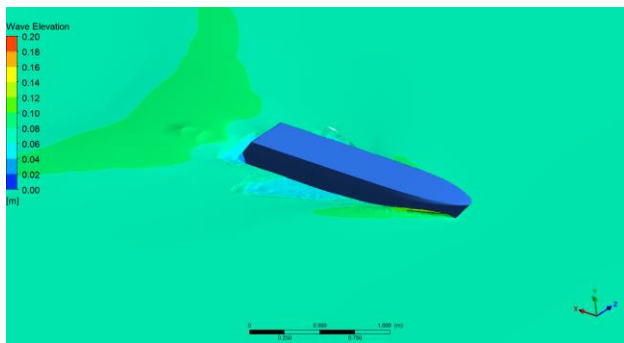**Figure 11.** Lateral pressure distribution at 0.1L from stern of bottom at Fr = 0.5

This event is not the cause of the difference in resistance in the two models. However, if you pay close attention, there are differences in the flow pattern behind the model which are quite different, in which the model without a tunnel (Figure 10.a.i)) has a pooled flow which causes the hull pull to be greater while in the model with a tunnel (Figure 10.a.i)) 10.a.ii) the flow pattern behind the model is more pointed which shows a more directed fluid flow and provides a reduced drag of the fluid against the hull of the model ship.

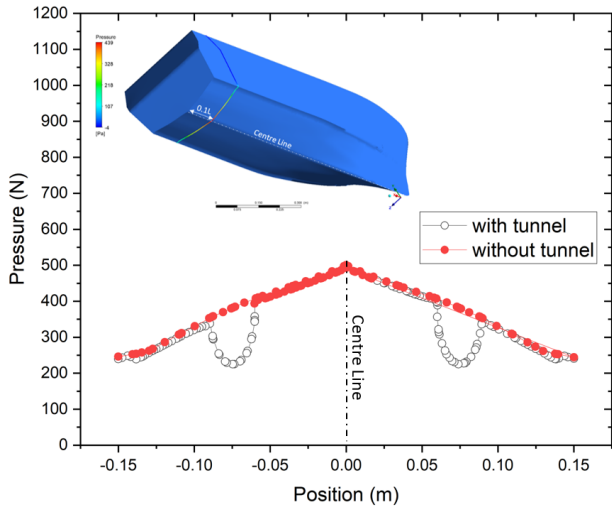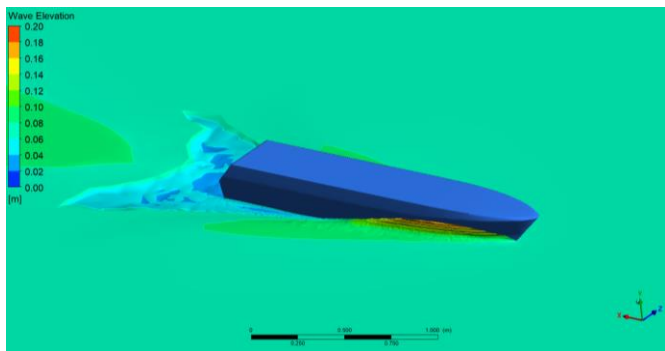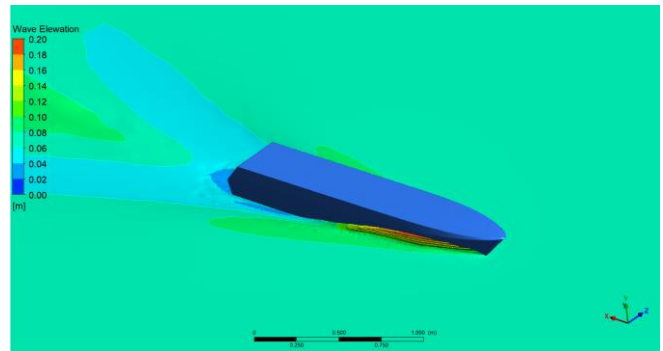The increase in pressure that builds up on the bottom of the two different models of fast patrol boats is proportional to the decline in resistance that takes place there. Both models exhibit a pressure distribution trend that is comparable to one another, but there is a difference of approximately 4.23% between the fast patrol boat model with tunnels and the fast patrol boat model without tunnels in terms of the pressure distribution value, as demonstrated in Figures 10.b and 11. The decrease in pressure in the tunnel, which has an average value of 9.71% as shown in Figure 11, is supporting evidence for the large reduction in drag that was observed. Additionally, the utilization of the tunnel on this rapid patrol boat results in a 7.2% overall reduction in drag when measured at a Fr of 0.8.

Conclusion

Numerical CFD research on the impact of tunnel changes on the Fast Patrol Boat model's resistance reduction has been conducted. The studies were conducted on a model of a rapid patrol boat with and without a tunnel. It is clear that CFD offers a significant contribution to the modelling and simulation of swift patrol boats. According to the calculations, rapid patrol boats with and without tunnels had a 5.4% reduction in resistance at CFD modelling findings. Load distribution trends are similar in both models, although the fast patrol boat model with tunnels has somewhat higher values than the fast patrol boat model without tunnels. The average pressure decrease in the tunnel is 7.71%, hence, this is supporting evidence for the reported resistance reduction.

Acknowledgements

References

[1] UNCLOS, Overview - Convention & Related Agreements, 1982. Available from: https://www.un.org/depts/los/convention_agreements/convention_overview_convention.htm (accessed Jan. 28, 2023).

[2] H. Ayu, Government Policy Directions on Illegal Unreported Unregulated (IUU) Fishing in Indonesia, in Internationalization of Islamic Higher Education Institutions Toward Global CompetitivenessSemarang, Indonesia – September 20th - 21th, 2018, 2018, pp. 106–114.

[3] Amkieltiela et al., The rapid expansion of Indonesia's marine protected area requires improvement in management effectiveness, *Mar. Policy*. **Vol. 146** (2022), p. 105257. DOI: 10.1016/j.marpol.2022.105257.

[4] Y. Listiyono, B. Pramono, L. Prakoso, K. Prihantoro, and D. Sianturi, Marine defense strategy in securing Indonesian archipelagic sea lanes (Alki) to realize maritime safety and maintain Indonesian soility, *Int. J. Educ. Soc. Sci. Res*. **04** (2021) 224–237. DOI: 10.37500/IJESSR.2021.4313.

[5] A. Lajeunesse, Canada's Arctic Offshore and Patrol Ships (AOPS): Their history and purpose, *Mar. Policy*. **124** (2021) p. 104323. DOI: 10.1016/j.marpol.2020.104323.

[6] F. Roshan, A. Dashtimanesh, and R. N. Bilandi, Hydrodynamic characteristics of tunneled planing hulls in calm water, *Brodogradnja*. **Vol 71, no. 1** (2020) 19–38. DOI: 10.21278/brod71102.

[7] V. A. Subramanian and P. V. V Subramanyam, Effect of tunnel on the resistance of high-speed planing craft, *J. Nav. Archit. Mar. Eng.* **Vol. 2, no. 1** (2005) 1–14 DOI: 10.3329/JNAME.V2I1.2025.

[8] M. Ghassabzadeh and H. Ghassemi, Automatic generation of the planning tunnel high speed craft hull form, *J. Mar. Sci. Appl.* **Vol. 11, no. 4** (2012). 453–461, Dec. 2012,
DOI: 10.1007/S11804-012-1155-9/METRICS.

[9] M. Ghassabzadeh and H. Ghassemi, An innovative method for parametric design of planing tunnel vessel Hull form, Ocean Eng. **60** (2013) 14–27.
DOI: 10.1016/J.OCEANENG.2012.11.015.

[10] F. Roshan, A. Dashtimanesh, and R. N. Bilandi, Hydrodynamic Characteristics of Tunneled Planing Hulls in Calm Water, *Brodogradnja*. **Vol. 71, no. 1** (2020) pp. 19–38.
DOI: 10.21278/brod71102.

[11] I. K. A. P. Utama, W. D. Aryawan, A. Nasirudin, Sutiyo, and Yanuar, Numerical investigation into the pressure and flow velocity distributions of a slender-body catamaran due to viscous interference effects, *Int. J. Technol.* Vol. 12, no. 1 (2021) 149. DOI: 10.14716/ijtech.v12i1.4269.

[12] ANSYS, ANSYS CFX-Solver Theory Guide. Canonsburg, PA, USA: Ansys Inc, 2020.

[13] F. R. Menter, Zonal two equation κ-ω turbulence models for aerodynamic flows, in AIAA 23rd Fluid Dynamics, Plasmadynamics, and Lasers Conference, 1993, 1993.

[14] F. R. Menter, Two-equation eddy-viscosity turbulence models for engineering applications, *AIAA J*. **Vol. 32, no. 8** (1994) 1598–1605.
DOI: 10.2514/3.12149.

[15] J. E. Bardina, P. G. Huang, and T. J. Coakley, Turbulence modeling validation, testing, and development, *Nasa Tech. Memo.* (1997),
DOI: 10.2514/6.1997-2121.

[16] A. F. Molland, S. R. Turnock, and D. A. Hudson, Ship Resistance and Propulsion, Cambridge University Press, 2017.
DOI: 10.1017/9781316494196.

[17] I. K. A. P. Utama, Sutiyo, and I. K. Suastika, Experimental and numerical investigation into the effect of the axe-bow on the drag reduction of a trimaran configuration, *Int. J. Technol.* Vol. 12, no. 3 (2021) 527–538.
DOI: 10.14716/ijtech.v12i3.4659.

MICROPLASTIC CHARACTERISTIC FOUND IN GASTROINTESTINAL TRACT OF PELAGIC AND DEMERSAL FISHES IN TUBAN, EAST JAVA

Dewi Hidayati[1], Fauziyah[1], Aunurohim[1], Nova Maulidina Ashuri[1], Edwin Setiawan[1], Yeyes Mulyadi[2], Nur Syahroni[2], Marita Ika Joesidawati[3] and Suwarsih[3]

[1]Department of Biology, Institut Teknologi Sepuluh Nopember, Surabaya, Indonesia
[2]Department of Ocean Engineering, Faculty of Marine Technology, Institut Teknologi Sepuluh Nopember, Surabaya, Indonesia
[3]Study Program of Marine Science, Universitas PGRI Ronggolawe, Tuban, Indonesia

E-mail: dewi_hidayati@ymail.com

ABSTRACT

Regular monitoring of microplastics contamination in marine biota have been concerned in the world, since its tiny size can be swallowed direct or indirectly and lead health problems. Tuban waters is the one of Indonesia's coastal and marine fisheries areas with high risk of microplastic pollution due to their highly anthropogenic activities. We investigated the microplastic in the digestive tracts of pelagic and demersal fishes in Tuban sea waters. Microplastic in fish sample guts were observed under microscope and the type of polymer were examined using FT-IR. This study reveals that number of microplastic in digestive tract of pelagic fishes were higher than demersal fishes. The dominant form was fiber (62%) with black color and dominant size ranging from 100-500 µm (72%). The types of polymers found were polyethylene and polyamide.

Keyword: Demersal Fish, Pelagic Fish, Microplastic, Gastrointestinal Tract

Introduction

Tuban Regency is one of the coastal cities in East Java which has a beach length of ± 65 km. The coastal and marine area in Tuban Regency is the center of the economy, which is often used for marine transportation, nature conservation, marine cultivation, tourism, and fishing settlements. [1]. Moreover, the rapid industrial development in Tuban increasing urbanization that led the adverse impact of the pollution in coastal and marine environment.

A total of 4.8-12.7 million tonnes of plastic have been identified in the oceans [2]. Thus, an estimated 10% of the plastic ends up in the ocean [3]. The four plastic size classes identified were nano-, micro-, meso-, and macro plastic from fishing activities and other anthropogenic plastic waste. Microplastic is a type of plastic waste that is smaller than 5 mm and is grouped into 2 types, namely primary and secondary microplastics [4]. Primary microplastics can be found in cleaning products and pellets which are produced

as raw materials for plastic production. Whereas secondary microplastics are produced from the breakdown of larger plastic items. Microplastics from secondary sources are often associated with areas with high population density [5], The total population may generate the high microplastics concentrations in the aquatic systems [6]. Another study in the densely populated coastal area reported that microplastic fragments in sediment of coastal area mostly originated from the breakdown of larger plastic [7]. The discarded larger plastic waste such as carry bags, water mineral bottles, containers, construction materials and toys enter the marine environment will breakdown to be fragments or fiber and contaminate sea water body for very long periods [5][8].

The tiny size of microplastic particle may be ingested by zooplankton and through the food web will contaminated in fish body [9]. Microplastic translocation will occur across the digestive tract and gills and enter the circulatory system. Through blood

circulation, microplastics will enter various organs in fish [10]. If plastic particles accumulate in large numbers in the fish's body, microplastics can clog the digestive tract of the fish [11].

In previous studies, as many as 504 demersal and pelagic fish were studied, and 36.5% were found microplastics in their digestive tract [12]. Several types of demersal fish, such as grouper fish (Epinephelus areolatus) and Japanese threadfin bream (Nemipterus japonicus). As well as types of pelagic fish such as herring scad (Alepes vari) and cleftbelly trevally (Atropus atropos) have high economic value, especially at the fish auction place (TPI) in Tuban. [13]. Therefore, according to several previous studies, there is a possibility that these microplastics can be accidentally consumed by various types of fish in Indonesia. In addition, the consumption of microplastics found in the gastrointestinal tract of pelagic and demersal fish has differences in the amount of accumulation [9]. The main objective of this research is to identify the characters of microplastics in the gastrointestinal of pelagic and demersal fishes from the waters of Tuban and have economic value.

Methodology

Study Area and Sampling

This research was conducted in September 2019-March 2020. The fish samples of grouper fish (Epinephelus areolatus), Japanese threadfin bream (Nemipterus japonicus), herring scad (Alepes vari), and cleftbelly trevally (Atropus atropos) were collected from local Fish Market in Tuban. Observation of microplastic in fish gastrointestinal were carried out at Laboratory of Zoology and Animal Engineering Department of Biology, Faculty of Science and Data Analytics, Institut Teknologi Sepuluh Nopember, Surabaya. The FTIR analysis was carried out at the Material Characterization Laboratory, Department of Materials Engineering and Metallurgy, Faculty of Industrial Technology and Systems Engineering, Institut Teknologi Sepuluh Nopember, Surabaya.

Sample Preparation and Extraction

Collection and identification of fish samples

The morphometry of 40 fish samples included total length, standard length, head length and body width were measured, then the species were identified refer to Whitten et al. (1993). The fish samples consist of two species of demersal fishes i.e., grouper fish (Epinephelus areolatus), Japanese threadfin bream (Nemipterus japonicus); and two species of pelagic fishes i.e., herring scad (Alepes vari), and cleftbelly trevally (Atropus atropos), whereas 10 individuals in each species. Fish samples were placed in the cool box with temperature of 4oC prior to examined in the laboratory. Gastrointestinal tract sample of fishes were prepared and preserved with 4% formalin with ratio solution: the tissue volume was 3: 1 [14] [15].

Microplastics analysis in gastrointestinal tract

The preserved gastrointestinal tract was dissected and its content were extracted by diluted in the solution of NaCl [16]. The microplastics were observed under stereo microscope that connected with Camera Optilab Advance 2.2 and Computer. The presence of microplastic particles were analyzed visually based on the morphological characters of shape, color, and size. The microplastic particles are measured using Image Raster software [17]. Observation of microplastic types refers to the results of the morphological identification category of microplastics according to Virsek et al. [18].

Chemical composition analysis of the gastrointestinal tract of fish

Chemical composition analysis uses a special instrument, Fourier Transform Infra-Red (FTIR) Spectroscopy to determine the type of microplastic [19]. The FTIR reading of a carbon-based polymer can easily be drawn from different bond compositions by generating a unique spectrum that differentiates plastic particles from other organic and inorganic particles [15] and can provide a unique infrared spectrum for certain chemical bonds [20].

Data Analysis

The homogeneity of fish body size was analysed using SPSS v.23. [21].

Result and Discussion

Homogeneity of Fish Body size

The homogeneity test showed that total length and total weight of each species samples were homogenous.

Microplastic Content in the Gastrointestinal Tract of Pelagic and Demersal Fish in Tuban Sea Water

The results showed that pelagic and demersal fish obtained from the waters of the Tuban Sea accumulated microplastics in the gastrointestinal tract tissue. This is presumably because the coast of Tuban

Regency has a high potential for plastic pollution, with a coastline length of ± 65 km, various human activities ranging from industry, ports, fisheries (cultivation and fishing), tourism, and settlements indirectly as waste disposal materials [22].
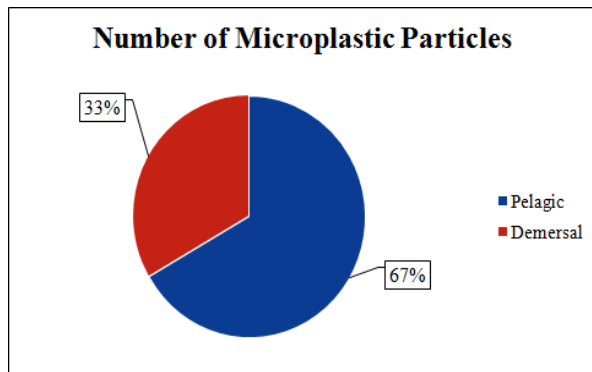
Figure 1. Total Number of Microplastics Found in Pelagic and Demersal Fish Species in Tuban Sea, East Java

Figure 1 exhibits that the percentage of accumulated microplastic particles in gastrointestinal of pelagic fish (67%) was higher than the in demersal fish (33%). This result is similar with the result reported by Rummel et al., whereas the ingestion frequency of microplastics in pelagic feeders significantly higher than demersal fish [23].

The results showed that the microplastics found in pelagic fish species were dominant in fiber and based on the FTIR test, the polymer yield was PE (Polyethylene) which had a lower density (ρ = 0.92 - 0.97 g/cm3) below the density of seawater (ρ = 1.027 g/cm3), causing microplastics to float in the waters and making microplastic consumption more in pelagic fish [24]. PE is the most widely produced polymer [25] and is also widely used for the packaging of products such as food containers and drinking water bottles. PE has also been used for textile fabrics as long and durable fibers [26], where the product can enter the sea through inappropriate wastewater treatment [27].

Physical and Chemical Characteristics of Microplastics in the Gastrointestinal Tract of Pelagic and Demersal Fish in Tuban Sea Waters

Color of Microplastic

The results of visual observations of microplastic color in the gastrointestinal tract of pelagic and demersal fish in the waters of the Tuban Sea found four types of MP colors including black, blue, red, and yellow (Figure 2 and Figure 3). The most dominant microplastic colors found in the gastrointestinal tract of pelagic and demersal fish were black followed by

blue, red, and yellow. The black color is caught by the fish because it is the same color as the pellet, and it is associated with some common prey [28].
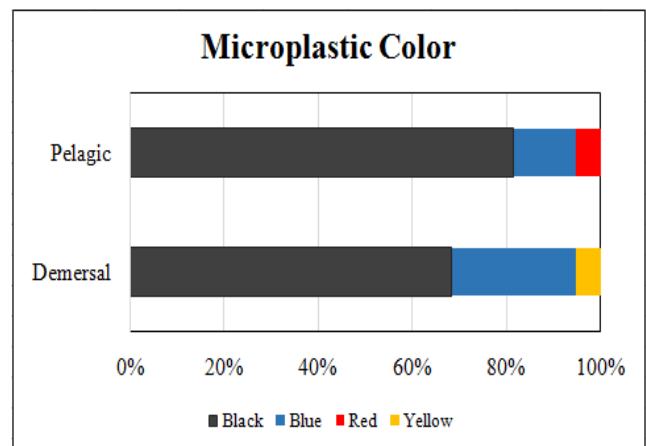
Figure 2. Percentage of Microplastic Color Found in Pelagic and Demersal Fish

Based on the FTIR test results, PE polymers are widely used. The source of this microplastics may be from daily packaging products such as grocery bags, plastic bags, food containers, and beverage bottles, causing the possibility of black, blue, red, and yellow microplastics coming from these products [26]. In addition, the black color is also thought to come from color degradation, where black microplastics are found in the gastrointestinal tract of old fish, basically because of their ability to absorb pollutants [29].
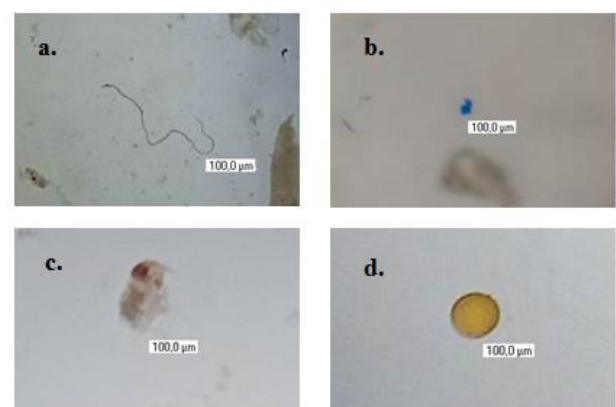
Figure 3. Color Variety of Microplastics Found in Gastrointestinal Tract of Pelagic and Demersal Fish in Tuban Sea Waters. (a) Black Fiber, (b) Blue Fragment, (c) Red Fragment, (d) Yellow Pellet

Shapes of Microplastic

The results showed that the dominant form of microplastic in pelagic fish was fiber (74%) followed by fragments (26%). Whereas, demersal fish were fiber (84%), fragments (11%), and pellets (5%) (Figure 4). The shape of the microplastics is shown in Figure 3. Shape variations in microplastics are caused by

degradation or erosion of the particle surface resulting from biological damage, photodegradation, chemical weathering, or physical effects (wave action, wind, weather-UV [5].
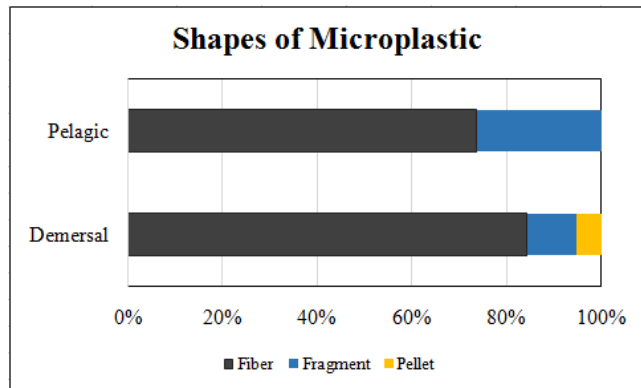
Figure 4. The percentage of Microplastic Shapes Found in the Gastrointestinal tract of Pelagic and Demersal Fish in Tuban Sea Waters

The FTIR test results showed that PA and PE polymers were found in the microplastic fiber. Previous studies have also suggested that the fiber usually consists of polymer acrylic, polyester, or polyamide (PA) [26]. This is due to the cloth washing process can release 1900-700,000 fibers per 6 kg into the environment [30]. The main fiber pollutants come from household waste as a consequence of washing cloth and daily use of personal care products [31] consisting of PE and PA polymers in the manufacturing process [26]. So the dominant form of fiber in this study can be caused by these products. In addition, PA polymers are also often applied as fishing gear used by the fishing industry [32]. Thus, the type of fiber originating from fishermen's activities comes from degraded fishing nets [33]. Primarily, the discovery of the dominant fiber in the gastrointestinal tract of pelagic fish is due to its thin shape and size, which causes the fiber to often be found floating on the surface of the water. [34]. However, the fibers released from the sewerage pipes of the wastewater treatment plant can enter the surface water and eventually accumulate in the sediment [31], causing the microplastic fiber to be found in demersal fish species.

Size of Microplastic

The Figure 5 reveals that microplastics found in the gastrointestinal of tract of pelagic and demersal fish in the waters of the Tuban Sea were in various sizes. According to Nor and Obbard (2014), visually observed microplastic particles were categorized based on ten class sizes: class 1 (<20 μm); class 2 (20-40 μm); class 3 (40-60 μm); class 4 (60-80 μm); class 5; (80-100 μm); class 6 (100-500 μm); class 7 (500-1000

μm); class 8 (1000-2000 μm); class 9 (2000-5000 μm); and class 10 (> 5000 μm).

Figure 5. Various sizes of microplastics found in the gastrointestinal tract of pelagic and demersal fish in Tuban Seawaters

The most microplastic size range found in the gastrointestinal tract of pelagic and demersal fish in the waters of the Tuban Sea is 100-500 μm (0.1-0.5 mm), which is in class 6. Then followed by class 7 with a size of 500-1000 μm (0.5-1 mm) and class 8 (16%) with a size range of 1000-2000 μm (1-2 mm). The percentage difference of each microplastic size found in pelagic and demersal fish can be seen in Figure 6.
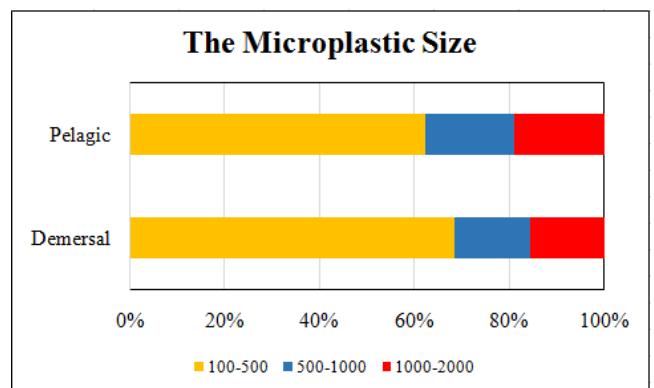
Figure 6. Percentage of Microplastic Size Found in Gastrointestinal Tract of Pelagic and Demersal Fish in Tuban Seawaters

Microplastic size can be affected by retention in fish bodies [35]. The greater the size of the gastrointestinal tract, the longer it is due to the difficulty of the egestion process. The small size of the microplastics also indicates the possible length of the degradation process experienced in the environment caused by erosion, temperature, or photooxidation [29]. In the benthic zone, continuous friction with sediment constantly results in smaller particles that accumulate on the ocean floor [36]. Based on the type of PA polymer detected in the fiber, it is likely that the source of the microplastic would be fishing gear [35].

Polymer type

The type of microplastic polymer was identified through functional group analysis of the sample using Fourier Transform Infrared Spectroscopy (FTIR). The analysis showed that the microplastic black fiber and

blue fiber have polymer types of polyethylene (PE) and polyamide (PA). Whereas the type of polymer identified in the blue fragment microplastics, and pellets is polyethylene (PE). These polymers are the most widely produced by the plastics industry and are often found in different marine environments around the world [27].

PE polymers are the main type of plastic observed in the gastrointestinal tracts of fish from fishing grounds, markets, beaches, and oceans [37; 38] and have been identified as the most polluting in aquatic environments due to their durability and various applications in packaging [39]. PE has a low density, so it is often found in pelagic fish [12]. In addition, PE is widely used in daily necessities [40]. PE polymer has a polyethylene density (ρ = 0.92 g / cm3) below the density of seawater (ρ = 1.027 g / cm3), causing the microplastics to float in the water column [24]. However, polyethylene polymers are also found in sediments because they are caused by biofouling [30].

Polyamide (PA) polymer type is the most common variety of thermoplastic polyester known as nylon, which is a useful raw material with high-strength fibers [28]. In addition, the use of polyamide is also applied in the manufacture of bearings, machinery and cooking utensils, fishing nets, and ropes [32].

Conclusion

The gastrointestinal tract of pelagic fishes (A. vari and A.atropos) and demersal fishes (E. areolatus and N. japonicus) from the waters of the Tuban Sea, East Java were contaminated microplastics with a percentage of 67% and 33%, respectively. The visual character of microplastics shows that the dominant color of microplastics is black, with the dominant shape of fiber and the maximum size ranging from 100-500 μm. The polymer types found in 4 of the 57 microplastic particles are polyethylene and polyamide.

References

[1] B. Damaianto dan A. Masduqi, Indeks Pencemaran air laut pantai utara Kabupaten Tuban dengan parameter logam, *Jurnal Teknik POMITS*. **Vol. 3, no. 1** (2014) 2337-3539.

[2] M. Haward, Plastic pollution of the world's seas and oceans as a contemporary challenge in ocean governance, *Nature communications.* **Vol. 9, no. 1 (2018)** 1-3.

[3] C. M. Free, O. P. Jensen, S. A. Mason, M. Eriksen, N. J. Williamson, dan B. Boldgiv, High-levels of microplastic pollution in a large, remote, mountain lake, *Marine Pollution Bulletin*. **Vol. 85, no. 1** (2014) 156-163.

[4] H. Hiwari, Noir, P. P., Yudin, N. I., Lintang, P. S. Y., dan Putri, G. M., Kondisi sampah mikroplastik di permukaan air laut sekitar Kupang dan Rote, Provinsi Nusa Tenggara Timur. **Vol. 5, no. 2** (2019) 165-171.

[5] V. Hidalgo-Ruz, Lars, G., Richard, C. T., and Martin, T., Microplastics in the marine environment: A review of the methods used for identification and quantification, *Environmental Science and Technology*. **46** (2012) 3060-3075.

[6] Collet I and Engelbert A, Coastal regions: People living along the coastline, integration of NUTS 2010 and latest population grid. *Statistics in Focus.* **30** (2013).

[7] Ni'am A.C, Hassan F, Ruei-Feng Shiu and Jheng-Jie Jiang, Microplastics in Sediments of East Surabaya, Indonesia: Regional Characteristics and Potential Risks, 2022.

[8] [8]. Hanun J.H, Hassan F and Sidik F, Indonesia Post-Pandemic Outlook: Environment and Technology Role for Indonesia Development The Existence of Microplastics as an Emerging Concern in Daily Routines and the Implications of Global Mitigation Efforts, 2022.

[9] O. Guven, Kerem, G., Boris, J., dan Ahmet, E. K., Microplastic Litter Composition of The Turkish Territorial Waters of The Mediterranean Sea, and Its Occurance in The Gastrointestinal Tract of Fish, *Environmental Pollution*. **30** (2017) 1-9.

[10] B. M. Rao, Microplastics in the aquatic environment: Implications for post-harvest fish quality, *Indian Journal Fish*. **Vol. 66, no. 1** (2019) 142-152.

[11] M. A. Browne, Stewart, J. N., Tamara, S. G., Steve, J. R., dan Richard, C. T., Microplastic moves pollutants and additives to worms, reducing functions linked to health and biodiversity, *Current Biology*. **23** (2013) 2388-2392.

[12] A. L. Lusher, Mchugh, M., dan Thompson, R. C., Occurrence of microplastics in the gastrointestinal tract of pelagic and demersal fish from the English Channel, *Marine Pollution Bulletin*. **Vol. 67 no. 1-2** (2013) 94-99.

[13] N. Wulan, Faktor-faktor yang mempengaruhi tengkulak ikan kecamatan palang kabupaten tuban memilih ikan dari tempat pelelangan ikan

(TPI) Kecamatan Brondong Kabupaten Lamongan, *Skripsi*. **Vol. 2, no. 3** (2013) 159-166.

[14] F. M. Baalkhuyur, El-Jawaher, A. B. D., Manal, E. A. E., Nabeel, M. A., Abdulaziz, M. A., Anders, R., Darren, J. C., Michael, L. B., dan Carlos, M. D., Microplastic in The Gastrointestinal tract of fishes along The Saudi Arabian red sea coast, *Marine Pollution Bulletin*. **131** (2018) 407-415.

[15] A. R. Hastuti, Lumbanbatu, D. T., and Wardiatno, Y., The presence of microplastics in the digestive tract of commercial fishes off Pantai Indah Kapuk coast, Jakarta, Indonesia, *Biodiversitas Journal of Biological Diversity*. **Vol 20, no. 5** (2019) 1233-1242.

[16] C. I. Yudhantari, Hendrawan, I. G., dan Puspitha, N. L. P. R., Kandungan mikroplastik pada saluran pencernaan ikan lemuru protolan (*Sardinella Lemuru*) hasil tangkapan di selat Bali, *Journal of Marine Research and Technology*. **Vol. 2, no. 2** (2018) 48-52.

[17] Anu, O., Rampe, H. L., dan Pelealu, J. J., Struktur *Sel Epidermis dan Stomata Daun Beberapa Tumbuhan Suku* Euphorbiaceae, *Jurnal MIPA UNSTRAT* (Online). **Vol. 6, no. 1** (2017) 69-73.

[18] Virsek, M.K., Palatinus, A., Koren, S., Peterlin, M., Horvat, P., Krzan, A., Protocol for microplastics sampling on the sea surface and sample analysis. J. Vis. Exp. **118** (2016) 1-9

[19] Kristina Borg Olesen, Nikki an Alst, Marta Simon, Alvise Vianello, Fan Liu, Jes Vollertsen and Mustafa Kansiz, Analysis of microplastics using ftir imaging identifying and quantifying microplastics in wastewater, sediment and fauna, Department of Civil Engineering, Aalborg University, Denmark Agilent, Australia.

[20] W. Wang and J. Wang, Investigation of microplastics in aquatic environments: An overview of the methods used, from field sampling to laboratory analysis, *Trends in Analytical Chemistry*. **108** (2018) 195-202.

[21] A. Field, Discovering Statistics Using SPSS, 3rd Edition, London: Sage, 2009.

[22] M. I. Joesidawati, Pencemaran Mikroplastik di Sepanjang Pantai Kabupaten Tuban, Prosiding Seminar Nasional Hasil Penelitian dan Pengabdian Kepada Masyarakat, Universitas PGRI Ronggolawe Tuban. **Vol 3** (2018) 8-15.

[23] C.D. Rummel, M.G.J.Lödera, N. F. Frickeb. T. Lang, E. Griebeler, M Janke and G. Gerdts, Plastic ingestion by pelagic and demersal fish from the North Sea and Baltic Sea, *Mar. Pollut. Bull*. (2016)

[24] UNEP, Marine Litter: An Analytical Overview. Nairobi: United Nations Environment Programme, 2005.

[25] G. Erni-Cassola, Vinko, Z., Matthew, I. G., dan Joseph, A. C., Distribution of plastic polymer types in the environment; A Meta-Analysis, *Journal of Hazardous Materials*. 369 (2019) 691-698.

[26] P. M. Silva dan M. A. Nanny, Impact of microplastic fibers from the degradation of nonwoven synthetic textiles to the magdalena river water column and river sediments by the city of Neiva, Huila (Colombia), *Water*. **Vol. 12, no. 4** (2020) 1-16, 2020.

[27] C. Lopes, Raimundo, J., Caetano, M., and Garrido, S., Microplastic ingestion and diet composition of planktivorous fish, limnology and oceanography letters. **Vol. 5, no. 1** (2020) 103-112.

[28] N. C. Ory, Gallardo, C., Lenz, M., dan Thiel, M., Capture, swallowing, and egestion of microplastics by a planktivorous juvenile fish, *Environmental Pollution*. **240** (2018) 566-573.

[29] N. Suwartiningsih, Setyowati, I., and Astuti, R., Microplastics in pelagic and demersal fishes of pantai baron, Yogyakarta, Indonesia, *Jurnal Biodjati*, **Vol. 5, no. 1** (2020) 33-49.

[30] M. Firdaus, Trihadiningrum, Y., and Lestari, P., Microplastic pollution in the sediment of Jagir Estuary, Surabaya City, Indonesia, *Marine Pollution Bulletin*. **150** (2020) 1-9.

[31] X. Wen, Du, C., Xu, P., Zeng, G., Huang, D., Yin, L., Yin, Q., Hu, L., Wan, J., Zhang, J., Tan, S., dan Deng, R., Microplastic pollution in surface sediments of urban water areas in Changsha, China: Abundance, composition, surface textures, *Marine Pollution Bulletin*. **136** (2018) 414-423.

[32] E. Hansen, Nilsson, N.H., Lithner, D., Lassen, C., Hazardous Substances in Plastic Materials. Denmark: COWI & Danish Technological Institute, 2013.

[33] M. R. Ismail, Lewaru, M. W., dan Prihadi, D. J., Microplastics ingestion by fish in the Pangandaran bay, Indonesia, World News of Natural Sciences, *An International Sientific Journal*. **23** (2019) 173-181.

[34] C. I. Yudhantari, Hendrawan, I. G., and Puspitha, N. L. P. R., Kandungan Mikroplastik Pada Saluran Pencernaan Ikan Lemuru Protolan *(Sardinella Lemuru)* hasil tangkapan di selat Bali, *Journal of*

Marine Research and Technology. **Vol. 2, no. 2** (2018) 48-52.

[35] D. Eerkes-Medrano and R. Thompson, Occurence, fate, and effect of microplastics in freshwater systems, *Microplastics Contamination in Aquatic Environments*. **4** (2018) 95-132.

[36] J. P. Da Costa, Santos, P. S., Duarte, A. C., dan Rocha-Santos, T., (Nano) plastics in The environment–sources, fates and effects, *Science of The Total Environment*. 566 (2016) 15-26.

[37] S. Karbalaei, Golieskardi, A., Hamzah, H. B., Abdulwahid, S., Hanachi, P., Walker, T. R., dan Karami, A., Abundance and characteristics of microplastics in commercial marine fish from Malaysia, *Marine Pollution Bulletin.* **148** (2019) 5-15.

[38] E. G. Cassola, Zadjelovic, V., Gibson, M. I., dan Christie-Oleza, J. A., Distribution of plastic polymer types in the marine environment; a meta-analysis," *Journal of Hazardous Materials*. **369** (2019) 691-698.

[39] R. A. Naik, Rowles III, L. S., Hossain, A. I., Yen, M., Aldossary, R. M., Apul, O. G., Conkle, J dan Saleh, N. B., Microplastic particle versus fiber generation during photo-transformation in simulated seawater, *Science of The Total Environment.* (2020)

[40] Hassan Namazi, Polymers in our daily life, *Bioimpacts*. Vol. 7, no. 2 (2017).

DESIGNING A BOAT HOTEL (BOTEL) FOR MARINE TOURISM ON TABUHAN ISLAND, BANYUWANGI REGENCY, EAST JAVA

Hasanudin[1], Ahmad Nasirudin[1], and Aditya Dwi Saputra[1]

[1]Department of Naval Architecture, Faculty of Marine Technology, Institut Teknologi Sepuluh Nopember (ITS), Surabaya, Indonesia
E-mail: hasanudin@na.its.ac.id

ABSTRACT

Tabuhan Island is one of the tourist islands in Banyuwangi Regency, which in 2020 was proclaimed by the Banyuwangi Regency government to become an international tourist destination. One of the efforts needed to make an international-class destination is to complete tourist objects with good infrastructure. One of the infrastructures that need to be completed is resorts and hotels. Design of Boat Hotel Catamaran (Botel Catamaran) is innovated with facilities equivalent to a 3-star hotel following the Ministry of Tourism and Creative Economy standards. This selection uses general dimension design parameters, which are then used in extensive travel and Botel facilities. Based on the calculations, the converted resistance of the engine has met the required power of 156 Hp. In addition, the calculation of the displacement-weight difference also showed a result of <9%, meeting the small ship margin requirement. The trim calculation also met SOLAS regulations with a result of 0% LWl < trim < 0.5% LWl. The freeboard calculation also met NCVS regulations with a result of Fb<(H-T). The tonnage calculation showed GT<500 GT, allowing the application of NCVS regulations. Finally, the comfort calculation (MSI) met the applicable ISO regulations. With these standardized calculation results, the engine is expected to operate optimally and safely. It was found that this ship has the final main dimensions, namely LoA = 29.26 m; Lpp = 28 m; B = 11.5 m; Height = 4 m; T=1.1m; B1 = 2.77; S = 6 m2 with a total of 6 rooms with a size of 30 m2 each and has been equipped with a restaurant and lounge. Then, the outline plan, general plan, and 3D model are drawn.

Keyword: Tourism, Tabuhan Island, BoTel, Catamaran

Introduction

Tourism is a potential resource that significantly contributes to Indonesia's development. However, it faces several obstacles, such as financing, promotion, and natural disasters, resulting in poor management. Therefore, this study aims to identify tourist attractions in Banyuwangi Regency, a newly developing district in Indonesia [1]. Banyuwangi Regency is located on the eastern tip of Java Island and offers a wide variety of natural tourist destinations, especially those related to nature tourism. Tabuhan Island is one of this district's most promising marine tourism destinations. It is an uninhabited island in Bengkak, Wongsorejo District, Banyuwangi Regency, East Java, and lies in the Bali Strait. This island is renowned for its white sandy beaches, clear light blue sea, shady trees, and breathtaking sunset and sunrise panoramas.

Furthermore, the island features beautiful coral reef spots, making it an ideal location for diving and snorkeling [2].

Figure 1. Tourism Tabuhan Island [3]

The Banyuwangi Regency plans to develop Tabuhan Island into a world-class destination with unique resorts that maintain local wisdom. This development will be done through partnerships with private

companies from abroad through a leasing agreement system [4].

Boat hotels have become a new tourist attraction developed by several researchers. The concept of a boat hotel allows tourists to stay overnight on a ship and enjoy the beauty of the surrounding sea. BoaTel appeals to tourists who want to experience a different kind of stay and connect with nature. The concept of boat hotels has been implemented in several countries, including at the Canal du Faux-Rempart in Strasbourg, France [5]. The concept of boat hotels and environmentally friendly tourism has become a necessity and trend worldwide [6][7].

The traditional Boat Hotel concept, named Le Pirate Boatel, has long been present in Indonesia, located in Labuhan Bajo [8]. However, the traditional design has not yet paid attention to the knowledge of naval architecture and ship safety. Therefore, this research discusses a new Boat Hotel design that is safe, comfortable and uses the principles of Naval Architecture. The hull concept uses a catamaran to provide a spacious deck and safe stability in slightly choppy waters.

In this paper, BoTel is a vessel designed to serve the Ketapang Port to Tabuhan Island in Banyuwangi. It adopts the BoTel design, which has been modified to meet the needs of maritime tourism in Indonesia. BoTel is designed to meet safety, security, and comfort standards according to passenger ship design standards. With its unique design and modifications, BoTel is expected to provide passengers with a comfortable and enjoyable travel experience while ensuring their safety and well-being.

Methodology

This research focuses on the location of marine tourism on Tabuhan Island, which was chosen for its international tourism potential. The construction of hotel facilities could improve the tourism standards in the area. Additionally, the waters around the island are characterized by calm and shallow conditions.

Research methodology is a framework to obtain accurate results following the research objectives. A structured and systematic research methodology is essential, as it can help researchers formulate problems, collect data, perform data analysis, and draw relevant conclusions. In research, a research methodology is created, which consists of several stages that must be carried out in a structured and sequential manner as figure 3.

Figure 2. Tabuhan Island Site [3]
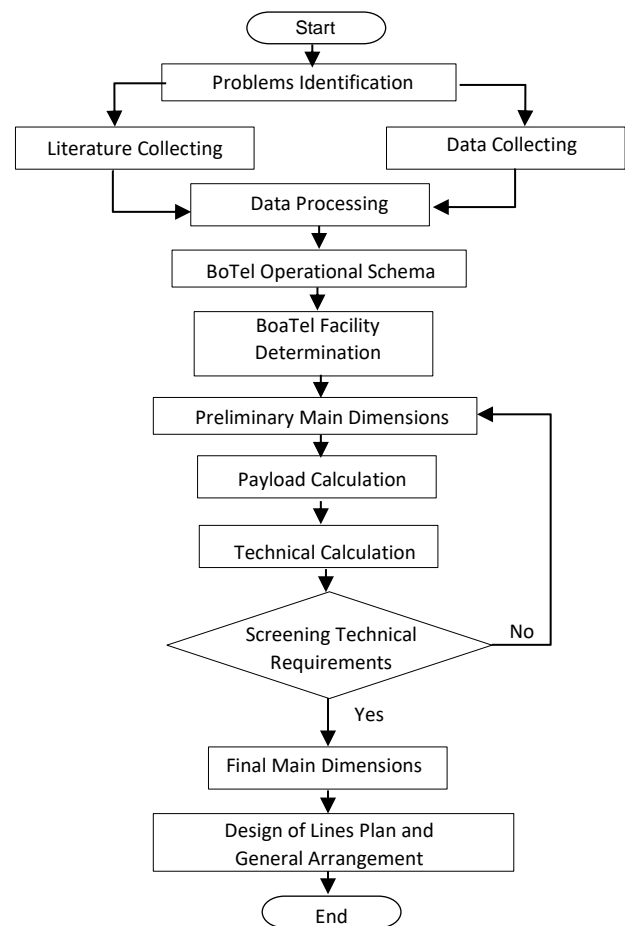
Figure 3. Flowchart of Research Methodology

Determination of Operational Scheme

The determination of the operational scheme is based on the natural conditions surrounding Tabuhan Island. Data on the island's natural conditions, such as its potential for superior tourism, is obtained from location surveys and literature studies. Based on this data, the best possible operational scheme for the ship can be determined. The results of the operational scheme can then be used in the following analysis.

Facility Determination for the Hotel

Before creating general and 3D plans, it is vital to determine the facilities that will be provided at Botel-Cat. This determination will affect the size of the building area above the main deck. The determination is based on standard hospitality rules issued by the Ministry of Creative Economy. The rules consist of two criteria: absolute and non-absolute. Due to the limited space on the ship, the focus will be on meeting the absolute criteria first in the ship's design [9].

Determination of Main Dimensions

At this stage, it is necessary to determine the depth of the water where the ship is anchored to set limits for its dimensions. The Parametric Design Approach method is used for this purpose, where researchers can decide the initial main dimensions of the ship. The primary size data is then divided into the first main dimensions and optimized through a spiral design process. The main dimensions that are decided include length (L), width (B), height (H), draft (T), mono-hull width (B1), width between demi hulls (S), and ship speed (Vs).

Payload Determination

The determination of the ship payload is based on the room space obtained from the facility plot method relative to the initial ship size. This plot will indicate the hotel rooms required to accommodate the passengers on the ship.

Determination of Technical Calculations:

The technical calculation of the ship consists of the following steps:

- **Calculation of coefficients and ship ratios**

    Table 1. Main Dimension Ratio [11]

Ratio Main Dimension Comparison		
5,9 <	L / B1	< 11,1
6 <	L / H	< 11
0,7 <	B / H	< 4,1
0,19 <	S / L	< 0,51
0,9 <	S / B1	< 4,1
0,9 <	B1 / T	< 3,1
0,15 <	B1 / B	< 0,3

Geometry coefficient and primary dimension ratio are essential factors in determining a ship's characteristics. In the design of BoaTel, a catamaran hull with a geometry coefficient using a slender body is used to maximize the speed and stability of the ship. In addition, the primary dimension ratio of this ship follows the ratio of a catamaran hull based on the Molland ratio, which has been proven effective in improving the ship's performance. The ratio limit is as table 1.

- **Calculation of resistance and ship power:** The resistance of a catamaran hull has two main components, namely the resistance of the two catamaran hulls and the interaction resistance between the two hulls. The resistance of the two catamaran hulls is calculated using the same formula as a mono-hull ship, which involves calculating the wetted surface area and the ship's speed. Meanwhile, the interaction resistance between the two hulls is calculated based on the distance between them and the turbulence effect between them. The formula used to calculate the resistance of a catamaran hull is formulated as follows [11]:

$$R_T = 0.5 \times WSA \times V^2 \times C_{tot} \qquad (1)$$

$$C_{tot} = (1 + \beta k) \times C_f + \tau \times C_w \qquad (2)$$

After calculating the ship's resistance, the results can be converted into the required power of the main engine needed to achieve the desired speed. The appropriate main engine can then be searched for in the main engine catalog based on the calculated power requirement for the ship.

- **Calculation of weight margin:** The displacement of a ship is an essential component in marine engineering as it determines the ability of a ship to float on water. The weight of a ship consists of two main components, namely, the weight of steel (W_L) and the dead weight tonnage (DWT). The weight of steel refers to the weight of the ship's steel structure, while the dead weight tonnage refers to the weight of the cargo or goods that can be carried by the ship. The weight components can be formulated as follows:

$$\Delta = W = W_L + DWT \qquad (3)$$

$$\Delta = (W_L + W_M + R)$$
$$+ (W_{Lo} + W_F + W_{PR} + W_P + W_{CR} + B) \qquad (4)$$

The weight margin of a ship is given as an allowance or reserve weight for the ship because not all components are accounted for during construction, and often there are additions. This margin ensures that the ship can still float and operate safely. The weight margin is usually set at less than 10% of the calculated ship weight for small ships.

- **Calculation of ship trim:** this is the condition where a ship has a difference in elevation between the bow and the stern waterline. Trim is calculated so that the ship's propeller is permanently submerged in water while sailing, allowing the engine to operate efficiently and increase the ship's speed. Ship trim is calculated using the provisions of SOLAS Chapter II-1, Part B-1, Regulation 5-1, which ensures that the ship has the appropriate trim for its characteristics and meets established maritime safety requirements.

$$0\% \text{ Lwl} \leq (Ta - Tf) \leq 0.5\% \text{ Lwl} \qquad (4)$$

- **Calculation of ship tonnage:** the tonnage of a ship refers to the maximum load capacity that a ship can carry. The tonnage of a ship is calculated based on the volume of enclosed spaces and the number of passengers or cargo that can be carried by the ship. The calculation of ship tonnage is critical because it will affect the safety requirements and equipment that must be met by the ship, including the number and types of safety equipment such as lifeboats and life jackets, as well as other requirements such as speed and distance between other ships at sea [10]. The formula for calculating tonnage is as follows:

$$GT = K_1 \times V \qquad (5)$$

$$NT = a + K_3 \times \left(N_1 \times \frac{N_1}{10}\right) \qquad (6)$$

- **Calculation of freeboard:** this is the vertical distance between the waterline and the main deck of a ship. A sufficient freeboard provides adequate reserve buoyancy to ensure the ship can sail safely, especially in rough weather conditions. The calculation of the freeboard can be done using various NCVS regulations. The formula for calculating freeboard is as follows.

$$Fb > (H - T) \qquad (5)$$

- Calculation of ship stability: this is one of the measures of a ship's safety that indicates the possibility of the ship capsizing. Stability is measured by the restoring moment arm (GZ), a function of the heel angle. The greater the value of GZ at a heel angle, the greater the restoring moment arm of the ship, making the ship more stable. The calculation of stability uses the following formula:

$$GZ(\theta) = GZ_0(\theta)^1 + GZ_{10}(\theta)^2 + \cdots \\ + GZ_{Vanishing}(\theta)^n \qquad (5)$$

- **Comfort Analysis:** A comfort analysis is performed to determine the level of passenger comfort. The comfort indicator used is Motion Sickness Incidence (MSI). The analysis is designed so that the ship is in a sea state condition that does not cause sea sickness for passengers. The calculation of MSI uses the following formula:

$$MSI(\omega_{e\ centre}) = \int_{\omega_{e1}}^{\omega_{e2}} S_{vert\ accel}(\omega_e) d\omega_e \qquad (6)$$

Linesplan Drawing

After obtaining the calculation results, the Botel-Cat design is drawn, which consists of a Lines Plan. This drawing must refer to the results of the main dimensions and technical calculations. The drawing process is assisted by CAD software.

General Arrangement and 3D drawing

Drawing the General Arrangement (GA) follows the planning of equipment and supplies used on the ship and the lines plan. CAD software applications assist the GA drawing process. Drawing the 3D design refers to the GA drawing with the help of 3D modeling software.

Result and Discussion

Operational Scheme Determination

The ship is designed to meet the hotel facility standards set by the Ministry of Tourism and Creative Economy while also being adjusted to the ship's capabilities and the needs of tourists. The standard level of facilities used follows a 3-star hotel standard [9].

The Botel design includes a hotel building, signage, lobby, front office, public restrooms, dining, and drinking facilities, guest bedrooms, kitchen, utilities, waste management, housekeeping, dining, and drinking areas, and health facilities. The operation distance between Mutiara Beach and Tabuhan Island is 1.62 nano miles. The ship is built to have a service speed of 7 knots. It can be reached in 15 minutes, twice as fast as a conventional existing boat.

The ship is designed to accommodate 12 passengers, determined by drawing the room layout on the ship's main deck while adhering to specified size limitations and minimum room area according to the chosen hotel type. The Botel Catamaran ship chosen is a 3-star hotel type, with consideration of the size and

hotel facilities that fit the ship's size. Based on the Regulation of the Minister of Tourism and Creative Economy on hotel business, the required number of crew members is determined to be ten, consisting of 4 crews and six non-marine crews.

Main Dimension and Ratio Determination

The main size of the ship is determined using the parametric design method. The ship's ladder is limited to 1.1 m based on the water depth around Tabuhan Island, where the ship is anchored. The main dimensions are obtained from mean ratios in Table 1 as follows:

Length perpendiculars (Lpp)	= 28	m
Breadth overall (B)	= 11.5	m
Height (H)	= 4	m
Draft (T)	= 1.1	m
S(m)	= 6.0	m
Breadth Demi Hull (B1)	= (B-S)/2	
	= 2.75	m
Maximum Speed (Vmax)	= 10.0	knots
Service Speed (Vs)	= 7.0	knots

It is essential to note the significance of these results and their implications for the design and operation of the ship. However, it is also important to avoid extensive citations and discussion of published literature and instead focus on the practical applications and implications of the results. A combined Result and Discussion section can help achieve this goal.

The Catamaran hull's performance depends on the ratio of its main dimensions, such as length, width, and height. Designers should consider ratios like length-to-beam, beam-to-draft, and length-to-draft to optimize stability, speed, and fuel efficiency. The ratios improve performance and reduce accidents at sea—the main dimensions ratio values are as follows.

Table 2. Checking Main Dimension Ratio [11]

Main Dimension Comparison				
L / B1	5,9 <	10,182	< 11,1	**Accepted**
L / H	6 <	7	< 11	**Accepted**
B / H	0,7 <	2,875	< 4,1	**Accepted**
S / L	0,19 <	0,214	< 0,51	**Accepted**
S / B1	0,9 <	2,182	< 4,1	**Accepted**
B1 / T	0,9 <	2,5	< 3,1	**Accepted**
B1 / B	0,15 <	0,239	< 0,3	**Accepted**

Machine Selection

The ship resistance calculation employs the theory of Insel and Molland because this particular ship falls within the scope of these calculations [11].

Consequently, the ship's resistance is determined to be 14.4 kN. Based on the known ship resistance, it is possible to calculate the necessary power and determine which main engine is suitable for this ship. In this case, two units of the Weichai WP4C120-18 engine, with the following specifications, are selected:

- Engine type: Weichai WP4C120-18
- MCR (kW): 120 HP (88 kW)
- Speed: 1800 rpm

To determine the power requirements for the ship's generator, the per-unit electricity needs of the ship are taken into account until the required electrical power value of 152.8 kW is reached. One engine requires 95.55 kW. As a result, the selected generator engine is:

- Engine type: Yxxxxr 4HAL2-TN
- MCR (kW): 156 HP (115 kW)
- Speed: 1800 rpm

Weight Calculation:

The method used for calculating a ship's weight and center of gravity involves breaking down the weight of the ship's skin and construction using a position-by-position method. Ship weight calculations consist of two parts: LWT and DWT. The ship's LWT is calculated by adding the weight of the ship, machinery, and Outfitting.

For this ship, the LWT is 70.61 tons. The DWT is calculated based on the consumables and the number of people on board. The DWT weight is 25.06 tons, making the ship's total weight 95.67 tons. The maximum acceptable difference between the ship weight and displacement is 10%. This ship's weight and displacement have a difference of 8.97%, which is within the acceptable limit, making it an acceptable ship.

Tonnage Calculation

The tonnage calculation formula refers to the Indonesian Flagged Non-Convention Vessel Standard (NCVS) [10]. As this ship design is classified as a small vessel for coastal crossing, the tonnage value of this ship is as follows:

- Gross Tonnage = 327.124 GT
- Net Tonnage = 98.137 NT

Since the NT value is greater than or equal to 0.3GT, it is accepted. Regulations to determine safety, stability, and freeboard for vessels with a GT value below 500 GT refer to NCVS regulations.

Stability Analysis

Ship stability refers to a vessel's ability to return to its original position after being affected by external disturbances, such as waves or wind, and its ability to avoid capsizing or overturning. The Maxsurf Stability Education Version software aids the stability analysis. According to the criteria established by the Non-Convection Vessel Standard (NCVS) [10], this ship meets the following criteria.

Table 3. Criteria stability of BoTel

Code		Criteria	Value	Units
NCVS Ch. 5A	Ch.5A - Comprehensive criteria of general application to all vessels	5A.3 - Area 0 to 40	5.1623	m.deg
		5A.6a - Initial GMt - Class 1	0.15	m.deg
NCVS Ch. 5B	Ch.5B - Alternative comprehensive criteria of general application to catamarans in operational areas B, C, D and E	5B.1- Area from 0 to 30	6.4996	m.deg
		5B.2 - Angle of maximum GZ	10	deg
		5B.3 & 4 - Angle of equilibrium - multiple heeling arms	16	deg
		5B.5: Area between GZ and HA	1.61	m.deg

Next, the stability calculations are compared to the stability criteria in **Table 4** for seven different load cases. The results indicate that all criteria for the seven load cases meet the following passing requirements.

Table 4. Stability of BoTel

No.	Load Case		5A.3	5A.6a	Status
	Penumpang	Consumables	(m.deg)	(m.deg)	
1	0%	10%	33.48	23.44	*Pass*
2	50%	10%	33.71	23.28	*Pass*
3	50%	50%	39.30	20.97	*Pass*
4	50%	100%	138.60	26.34	*Pass*
5	100%	10%	33.94	23.13	*Pass*
6	100%	50%	39.46	20.84	*Pass*
7	100%	100%	138.40	26.21	*Pass*

No.	Load Case		5B.1	5B.2	5B.3	5B.4	Status
	Penumpang	Consumables	(m.deg)	(deg)	(deg)	(m.deg)	
1	0%	10%	15.43	10.00	3.9	26.79	*Pass*
2	50%	10%	15.47	10.00	3.9	26.89	*Pass*
3	50%	50%	18.704	10.90	3.3	28.855	*Pass*
4	50%	100%	41.696	14.50	2.2	43.667	*Pass*
5	100%	10%	15.524	10.00	3.9	0.1	*Pass*
6	100%	50%	18.702	10.90	3.3	28.87	*Pass*
7	100%	100%	41.593	14.50	2.1	43.561	*Pass*

Comfort Analysis

The comfort analysis method utilizes Maxsurf Motion software by inputting required variables such as wave height, significance, heading, and desired location to analyze the MSI value [12]. In this study, the areas analyzed for comfort include passenger rooms 1 (front), 2 (middle), and 3 (back), crew accommodation room, restaurant, and lobby. These locations were selected based on the frequency of visits by passengers and crew. The variation of wave direction used against the ship's angle of incidence includes 0 degrees (following sea), 45 degrees (quartering sea), 90 degrees (beam sea), and 180 degrees (head sea).

The analysis was conducted in various areas where visitors spend their time, such as rooms, crew rooms, restaurants, and lobbies. The comfort standard is used for an operational time of 30 minutes, adjusted to the estimated time the ship sails on one trip. Based on the inputs, the results are presented in Figures 7, 8, 9, and 10. The results from the curves indicate that the encounter frequency value for all areas checked for comfort remains below the discomfort limit for a 30-minute cruise time (gray line). Therefore, it can be concluded that the Botel design provides good comfort.

Design of Lines Plan and General Arrangement

After obtaining all the necessary calculations, the ship's design can be finalized. The ship's design drawings include a Lines Plan, General Arrangement, and a 3D model. These drawings are created using Maxsurf Modeller, AutoCAD, and 3D modeling software. Figures 4, 5, 6, and 7 depict the Lines Plan, General Arrangement, and 3D model drawings.

Conclusion

Maritime tourism using fuel-efficient and environmentally friendly ships has become increasingly important worldwide. Various research and scientific publications have addressed this issue, including studies on using renewable energy in tourist ships, reducing carbon emissions in the shipping industry, and waste management strategies on tourist ships. This paper presents the design of the BoaTel ship, which is a development of previous research and meets the market demand on Tabuhan Island with the following results:

1. The operational scheme planning for the Botel Catamaran ship is as follows: the ship will sail from Mutiara Beach of Tabuhan Island to Tabuhan Island, with a maximum sailing time of

15 minutes. The ship will stay overnight on Tabuhan Island for 18 hours before sailing back to the initial departure point at Mutiara Beach Tabuhan,

2. The facilities on this ship have been established according to the standards set by the Ministry of Tourism and Creativity,
3. The main dimensions final of the BoTel are as follows: Loa = 29.26 m, Lwl = 28 m, B = 11.5 m, B1 = 2.75 m, H = 4 m, T = 1.1 m, S = 6 m, Vs = 7 knots, Crew = 10 persons, Passengers = 12 persons,
4. Design drawings of the line plan and general plan have been created to align with the characteristics of the Tabuhan Island waters.

Acknowledgements

References

[1] M. Murniati, G. Maski, I. Noor, and M. Ekawaty, Identification of tourism potential and investment strategy- a case study of Banyuwangi Regency, *EEA*. **Vol. 39, no. 12** (2021). DOI: 10.25115/eea.v39i12.6003.

[2] Tabuhan Island - Indonesia Travel. Available from:https://www.indonesia.travel/gb/en/destinations/java/banyuwangi/tabuhan-island

[3] Google Maps, Google Maps. https://www.google.co.id/maps/place/Pulau+Tabuhan/@-8.0372222,114.4611111,3a,87.5y,90t/data=!3m8!1e2!3m6!1sAF1QipPLRguctirck-YaKwoNngc9Ab2iF63dftjTZkOe!2e10!3e12!6shttps:%2F%2Flh5.googleusercontent.com%2Fp%2FAF1QipPLRguctirck-YaKwoNngc9Ab2iF63dftjTZkOe%3Dw153-h86-k-no!7i600!8i337!4m7!3m6!1s0x2dd13f6c4582f3d1:0x5a182cafde666aea!8m2!3d-8.0372222!4d114.4611111!10e5!16s%2Fg%2F11gznhdk1 (accessed Apr. 11, 2023).

[4] A. Fanani, Pulau Tabuhan Banyuwangi akan Jadi Destinasi Kelas Dunia, detiknews. Available from: https://news.detik.com/berita-jawa-timur/d-4861105/pulau-tabuhan-banyuwangi-akan-jadi-destinasi-kelas-dunia (accessed Apr. 11, 2023).

[5] J. Mehran and H. GT. Olya, Canal boat tourism: Application of complexity theory, *Journal of Retailing and Consumer Services*. **Vol. 53** (2020), p. 101954.

[6] M. A. A., S. C. Joseph, R. V. Chacko, A. Joseph, J. P. P., and D. P. Raghavan, LVDC Architecture for Energy Efficient House Boat Hotel Load System, in 2019 National Power Electronics Conference (NPEC), Tiruchirappalli, India: IEEE, Dec. 2019, pp. 1–5. DOI: 10.1109/NPEC47332.2019.9034835.

[7] A. Mohammed Ajlif, S. C. Joseph, P. P. Jayan, D. P. Raghavan, A. Joseph, and R. V. Chacko, Energy Efficient LVDC Architecture for House Boat Hotel Load System, in 2020 IEEE International Conference on Power Electronics, Smart Grid and Renewable Energy (PESGRE2020), Cochin, India: IEEE, Jan. 2020, pp. 1–5.

[8] Pujakesuma, 10 Rekomendasi Hotel Terbaik Untuk Menginap Dan Bermalam Di Labuhan Bajo. May 17, 2020. Available from: https://www.mediatravelling.com/2020/05/10-rekomendasi-hotel-terbaik-untuk.html (accessed Apr. 11, 2023).

[9] Kementerian Pariwisata dan Ekonomi Kreatif Republik Indonesia, Peraturan Menteri Pariwisata Dan Ekonomi Kreatif Republik Indonesia Nomor PM.53/HM.001/MPEK/2013 Tentang Standar Usaha Hotel.

[10] Indonesian Flagged Non Convention Vessel Standard Is Applied, Kementerian Perhubungan Republik Indonesia. Available from: https://dephub.go.id/post/read/standar-kapal-non-konvensi-kapal-berbendera-indonesia-mulai-berlaku-10439?language=id (accessed Apr. 12, 2023).

[11] M. Insel, An investigation into the resistance components of high speed displacement catamarans, PhD Thesis, University of Southampton, 1990.

[12] ISO 2631-1:1997, ISO. Available from https://www.iso.org/standard/7612.html (accessed April 12, 2023).

INTEGRATION ANALYSIS OF DRONE MULTI SENSOR-GNSS-LIDAR-CAMERA FOR 3D MAPPING (CASE STUDY: PT GARAM, PAMEKASAN, MADURA)

Daud Wahyu Imani[1], Mokhamad Nur Cahyadi[1], Imam Wahyu Farid[2], Ronny Mardianto[2]

[1] Geomatic Engineering, Sepuluh Nopember Institute of Technology, ITS Sukolilo Campus, Surabaya, Indonesia
[2] Electrical Engineering, Institut Teknologi Sepuluh Nopember, Surabaya, Indonesia

E-mail: cahyadi@geodesy.its.ac.id

ABSTRACT

Every year salt was carried out by PT Garam twice whereas the previous process used the method of terrestrial and manual calculations with sacks. Therefore, a map of salt production is needed using the Global Navigation Satellite System (GNSS) and Inertial Measurement Unit (IMU) sensor navigation system to increase the data's accuracy level. Unmanned Aerial Vehicle applications for the purpose of obtaining geometric documentation results and for capturing textures that characterize object structures. (Adamopoulos, 2020). LiDAR can classify based on the number of image acquisitions processed in the software, utilizing photogrammetric, and structural science principles from Motion technology. (Fernández, Hernandez et.al 2015) LiDAR Acquisition process that enables the creation of point clouds, three-dimensional models, and Digital Surface Models with high accuracy. (Barba, et al. 2019). A three-dimensional model makes it easy for users to choose a virtual position on the map, has good accuracy in interpreting the map, and displays a more real shape. LiDAR has a disadvantage in the form of coordinate data positions that have local references. (Cahyadi., et al. 2019). Unmanned Aerial Vehicle (UAV) technology has the advantage of efficiency in the cost and time of data collection. These researchers use multi-sensor technology GNSS, LiDAR, and Drones to map the stockpile of salt on open land and in warehouses. makes it easy to calculate the area of salt land and calculate the volume of salt production. This was done for PT GARAM to meet the community's needs and monitor the amount of salt production. This data can be used as a reference for digital asset inventory and the system can be applied to optimize the salt industry. The drones used in this study are the DJI Matrice 300 and the Low-Cost Drone Tarot Iron Man 650. Both types of drones are used to measure land and salt volume. The end product of the research is in the form of data generated in the form of a point cloud to calculate the salt stockpile volume and the elevation level of the salt land area.

Keyword: LiDAR, Salt, and Unmanned Aerial Vehicle

Introduction

PT. Salt (Persero) is a state-owned company engaged in salt production in Indonesia as an industry that produces the availability of national salt. PT. Salt, located on Madura Island, has an area of around 5,600 hectares spread across Sumenep Regency and Pamekasan. Optimization of salt production is needed because salt needs are related to various sectors. PT Garam has obstacles in the process of monitoring salt production. That is because salt is monitored and calculated manually with the help of sacks. The method has many shortcomings in the form of

inefficient time in calculating salt and the data accuracy level. Another method used to calculate the volume of salt is to use a total station. However, the tool has a shortage in terms of time efficiency because every point aim to require the mobilization of human resources in order to get accurate results. Therefore, in this study, UAV was used to accelerate the monitoring of salt land as a basis for conducting production calculations. This step is carried out because the area of salt land is directly proportional to salt production. In addition, UAVs make it easy to measure in areas with broad coverage and high

mobility. However, measurements with UAVs still have not answered the need to optimize salt production due to a lack of data accuracy to determine the elevation of salt land. The elevation is known to determine the distribution of land contours to optimize salt land production. Therefore, in this study, the integration of Lidar and UAV was carried out to make more effective measurements than the conventional methods that have been carried out. As for the GNSS tool, it is used to help UAV positioning when flying in the air. This measurement requires manufacturing salt production maps using the Global Navigation Satellite System (GNSS) and Inertial Measurement Unit (IMU) sensor navigation system.

Based on (Shao Zhenfeng, 2021), theoretically, the UAV platform (Unmanned Aerial Vehicle) and the mobile mapping vehicle platform can be equipped with high-temporal, high-spatial, and high-spectral resolution. UAV is used for remote sensing applications for urban areas as observation material achieved by building appropriate models or algorithms based on spatial, spectral, and shape features. Therefore, research was conducted by LiDAR using Pixhawk to integrate with the GPS. Based on the journal (Malberg, 2022), the measurement of salt stockpile volume can be done using LiDAR. The LiDAR uses a type of rotation Velodyne 30 degrees, 7 times the acquisition time, and 10 times the scanning length. The measurement method still has to adjust to the size and area to acquire some data en masse. Based on the data (Malberg, J.A 2022) obtained from the results of the camera acquisition, the next step is forming a digital surface model. Photo grids will be used as validation data with a grid area of 0.1 x 0.1 meters. This study uses a 360 Go Pro camera as a surface-matching material to adjust the shape of the existing salt stockpile. Lidar data acquisition has an estimated time of under 15 minutes. LiDAR can conduct classifications based on the number of image acquisitions processed in software, utilizing photogrammetry principles and motion technology structures (Fernández., et al., 2015). The LiDAR acquisition process allows the manufacturing of cloud points, and 3D models, with high -form density and accurate images. (Barba., Et al 2019). After the GPS measurement coordinates are obtained, georeferencing is carried out to integrate with the geographical information system. Lidar data obtained are processed in the Global Mapper application and Cloud Compare. The volume calculation process using conventional measurements in terrestrial methods

requires a long time and an enormous cost. Therefore, this research uses a combination of sensors such as GNSS Low Cost and LiDAR. GNSS Low Cost serves to give a position value to the observed object. Meanwhile, integrated LiDAR is used for 3D data collection for mapping purposes by getting the results of cloud points in coordinates X, Y, and Z. These results are then processed to determine the height at the measurement location.

LiDAR has a deficiency in terms of data coordinate positions obtained that have local references. Therefore, GPS helps determine the position of the data obtained to increase accuracy and get good data quality in terms of precision and accuracy. The main advantages of GNSS low-cost technology are the it hase geodetic type's quality. (Cahyadi., Et al 2019). GNSS technology, more commonly called the Global Positioning System technology, is a coordinate acquisition tool that produces latitude, longitude, time, and height data in scientific units on earth. (Taufik., Et al 2019) GPS Low-Cost technology experiences significant development at a low cost and a little use of energy, including producing data quality that has an accuracy equivalent to geodetic GPS. (Taufik., Et al 2019) The need for data acquisitions with GPS technology with the availability of more economic tools is inversely proportional because GPS technology has a price of around 2000 USD (Yuwono., et al., 2019). The GNSS-Mimu integration technique has been developed, such as by adding additional sensor tools in the form of pixhawk. The tool can make a three-dimensional model, making it easier for users to find the map's virtual position and better accuracy. The UAV application is used to get the results of geometric documentation and capture the texture that characterizes the object's structure. (Adamopoulos, 2020).

This study will calculate the volume and land stockpile of PT. GARAM in Pamekasan Regency. The drone has a maximum flying height of 120 meters from the surface and is integrated with the GNSS-LiDAR sensor to achieve accurate, fast, and inexpensive missions. In the research that will be conducted, UAV data will be used to calculate the volume of the land stockpile of PT. GARAM. The development of UAV, GNSS, and LiDAR technologies, combined into one newest technology to cover each other's deficiencies, aims to increase the accuracy of calculating the volume of PT. GARAM. LiDAR volume measurement validation data with elevation measurements using a Total Station and Waterpass. This study provides an overview of the

comparative analysis of Multi-Sensor Drone measurements with conventional terrestrial measurement methods with GPS and Total Stations reviewed through the time of measurement and the costs used in the period of taking the salt stockpile data that has been determined. This method speeds up the process of calculating the volume and stockpile of salt land both inside and outside the Warehouse. PT. Garam has 200 warehouses at the beginning and 200 at the end of the year, so this method is expected to speed up the stockpile evaluation completion process at PT Garam.

Methodology

This study used a Multisensor Drone to measure salt fields and calculate salt volume. The UAVs used consist of the DJI M300 and the Tarot Iron Man Drone for data acquisition. IPAD LiDAR technology is used to compare data with RP LiDAR A1 and Livox MID-40. The data used as validation is a triangular measurement in the form of Low-Cost GNSS and Total Station. In addition, there is supporting data, such as the results of interviews with PT GARAM partners. The following is a flow chart of the measurement methods that have been carried out.

Early stage

In the early stages, two activities were carried out in the form of field orientation and determining the measurement area. Field orientation aims to determine the characteristics of the land being measured. The next activity is determining the measurement area to determine the object's boundaries and the characteristics of the land being measured. In addition to getting to know the measurement area, the two activities were carried out to determine the measurement boundaries and the measurement method to use.

1. **Measurement Stage**

    Salt Land measurements are carried out in the warehouse with an estimated time of 1 week of data acquisition. Data validation was compared between the Low-Cost Drone Multi-sensor measurement results with the Terrestrial Total Station and LiDAR IPAD methods. Photogrammetry + LiDAR measurements are carried out by utilizing the Low-Cost Drone RTK instrument, which is integrated with the LiDAR device. This measurement aims to obtain coordinate data and obtain point clouds recorded by LiDAR devices. These measurements were

made to calculate the volume of the salt stockpile. The GNSS data recording was carried out to obtain validation coordinate values that are spread over the salt land measurement area. The method used in recording data using GNSS is the static method with the concept of net measurement and the Real Time Kinematic method for correcting the measurement results of the DJI M 300 LiDAR Livox MiD 40 Drone. Terrestrial measurements were carried out using a total station. This measurement aims to obtain the volume of salt in the warehouse, which will be used as a comparison value from the value obtained from photogrammetry + LiDAR measurements. IPAD measurements were carried out to obtain LiDAR data, coordinates, and three-dimensional visualization. Measurements using IPAD are carried out by circling the object to get the results of measuring the salt stockpile volume.

2. **Data Analysis Stage**

    The analysis stage is carried out to carry out measurement data validation tests between various methods. Primary data is the result of measurement, and secondary data is the result of validation from PT Garam Pamekasan. The georeferencing process is carried out to adjust the data results to the base map. In volume measurement, validation is carried out in the form of measurements using the terrestrial method in the salt cellar. Data distribution analysis used the standard deviation method to do filtering data signal outages. Field measurements and salt stockpile volumes used the RMS Error method to test the level of accuracy compared to the validation data.

IMU (Inertial Measurement Unit)

The Inertial Measurement Unit (IMU) is an inertial navigation system that became known in 1950 and is more accurate for terrestrial navigation purposes (Morton, 2021). An IMU equipped with a base navigation computer is called an INS (Inertial Navigation System). In this study, researchers used IMU because the data acquisition location was indoors, and the drone was flown manually. In addition, the use of IMU indoors plays a role in providing position information because the GPS signal indoors is weaker than in an open area. According to Groves (2008), the IMU generally consists of 2 sensors: the accelerometer and the gyroscope. Some

IMUs were developed incorporating additional inertial sensors to protect against single-sensor failure, but these sensors are more subject to inaccuracies due to temperature variations and bias (Jose, 2009). The specific force is the difference between the actual acceleration in space and the acceleration due to gravity, so the resulting acceleration is linear. The gyroscope is used to measure the orientation of a moving vehicle by providing an output in the form of angular velocity. The acceleration and speed information generated by the IMU can then be translated into position information, although this position information is less accurate than GPS (Groves, 2008). IMU is used to keep the drone able to fly indoors. In the Low-Cost Drone, there is a Pix Hawk type 2.4.8, which is used so that the quadcopter can fly stably. The tool is connected to Garmin GPS to help position the drone while flying. In addition, Pitch, Roll, and Yaw data are used to correct the position of the LiDAR object. The correction was made during the post-processing of the salt volume measurement results. Altitude, Longitude, and Latitude values are converted to UTM coordinates first. Before calculating, the LiDAR position rotated 90 degrees due to adjusting the LiDAR position during acquisition with Low-Cost drones. If the translation and rotation processes are not carried out during the object acquisition process, only the drone's flight path data can be plotted.

Algorithm

Precision and Accuracy

Several terms are used to describe measurement reliability, namely precision, accuracy, and uncertainty (Mikhail and Gracie, 1981). GNSS receiver requires a large area to receive signals from the satellites it tracks. If the receiver's line of sight to the satellite is blocked by objects such as buildings, trees, bridges, and other objects, the receiver cannot receive signals from the satellite. So the receiver cannot calculate its position or time. The solution for signal outages/blockage is the receiver tracking more than one constellation, or the user can integrate a GNSS receiver with several navigation sensors, such as an IMU. IMU can assist in bridging signal outages/blockages, such as those caused by objects such as buildings, trees, bridges, and others, and also in recovering GNSS signals after signal outages/blockages (Novatel inc, 2020). Precision is defined as the degree of closeness of repeated measurements to the same object. Accuracy is indicated by the spread of the data distribution. The smaller the distribution, the higher the accuracy, and vice versa. The usual size is the standard deviation. The higher the accuracy, the smaller the standard deviation value, and vice versa. Accuracy is the degree of closeness of the measurement results to the correct value. Correctness is not only the result of random error but also the bias that exists due to uncorrected systematic error. The precision value can be indicated by the standard deviation value of measurement and the Root Mean Square Error (RMSE) of the processed data. Accuracy tests were carried out to determine the accuracy of land measurements and the volume of salt stockpile made and were carried out based on each three-dimensional model space. The following is the formula for calculating equation 2.1 from the Root Mean Square Error (RMSE):

$$RMS=\sqrt{(\sum_{(i=1)}^{n} [n(X_{model}-X_{validation})^2])/n} \quad (2.1)$$

Explanation:

- $xmodel$ = Values on salt field measurement results
- $xvalidation$ = Value on total station validation data
- N = Lots of measurement samples

Based on the data processing results, there is a Standard Deviation Analysis to determine the distribution of data. Standard Deviation analysis is performed to filter data that experience data outages. Standard Deviation analysis is carried out while processing Salt Stockpile volume data. The following is the formula for equation 2.2 to calculate the standard deviation:

$$Deviation\ Standard=\sqrt{(\sum_{(i=1)}^{n}(n\ pop-pop\ average)^2)/n} \quad (2.2)$$

Explanation:

- n pop = The number of samples of measurement of Low-Cost Drone coordinates
- pop average = The results of the calculation of the average measurement results of Low-Cost Drones

Area Geometry

The area geometry accuracy test is carried out based on the standard error percentage value of less than 2% based on the Technical Specifications of the Regulation of the Minister of Agrarian Affairs (PMNA), Head of the National Land Agency (BPN) Number 3 of 1997 concerning tolerance of different percentages of land area. The formula used to calculate the percentage of area geometric errors is as follows:

% wide difference error = (x_model-x_validation)/x_validation × 100% (2.3)

Explanation:

- Xmodel = value in a three-dimensional model
- Xvalidation = value on validation data

Research sites

The construction of a multi-sensor drone using UAVs for land mapping on PT Garam's land aims to obtain altitude data. In addition, multi-sensor drones were also tested for 3D modeling. The objects that will be examined in this activity are several areas in PT Garam's land, especially in Pamekasan Regency. This location has coordinates 7.20055, 113.54906. The volume data acquired is in the Salt Transit Warehouse, with an area of 20 x 40 meters with an estimated height of 8 meters. The Transit Warehouse can accommodate around 2000 tons of salt.

Figure 1. Research Site

Measurement Data

Measurement data consists of validation data and measurement results data. The measurement results contain volume LiDAR Drone Data and PT Garam Pamekasan Stockpile Land. The validation data be composed of Raw Low-Cost GNSS measurement data and Total Station Measurement Result Data. Additional measurements were carried out to increase the variety of data using IPAD 2021. In addition, there are Secondary Data in the form of interview results from partners of PT Garam.

Low-Cost Drone Multi-Sensor

The Tarot 650 Iron Man drone is equipped with a payload system to carry payloads in the form of multi-sensors consisting of GNSS, LIDAR, and low-cost IMU LiDAR quadcopter-type drones that are more adaptive in maneuvering. The drone is equipped with a payload

box with a larger payload capacity than the low-cost drones that have been on the market before. This capacity allows the drone to carry multiple sensors at once.

Figure 2. Low-Cost Drone LiDAR Multi-Sensor

Based on Figure 2. GNSS sensor and RP LiDAR A1, the payload is also equipped with an IMU sensor and gimbal to support accurate positioning. LiDAR data acquisition is carried out between the two legs of the multi-sensor drone with a range of 140-220 degrees. Low-Cost Drone Components assembled:

1. Devices: bldc motor, esc, flight controller, GPS, USB, telemetry, transmitter, receiver, propeller, and 4s battery
2. Data acquisition range: Logitech c270 camera, maximum flight altitude of 12 meters, and 8 cm LiDAR detection capability
3. Estimated Price: 21,000,000
4. LiDAR file legend: Time; rolls; pitches; yaw; altitudes; latitude; longitude; compass; data Lidar (angle ranges 140-220)
5. Data Acquisition: Each corner has 2 data, so, at a measurement of 140-220 degrees (80 degrees), there are 160 data for each data collection.

RPLIDAR A1M8-R6 is a type of LiDAR that has an object scanning sensor using a 2D laser beam with a 360-degree angle. This LiDAR technology can scan within 12 meters and have a 360-degree angle range. The resulting data is in the 2D form, which can be used for mapping, localization, and environmental modeling. The RPLIDAR A1 scan frequency reaches 5.5 Hz and can scan up to 360 samples per round, and the frequency can be set up to a maximum of 10 Hz. The RPLIDAR A1 operates well in all types of indoor and outdoor environments without sunlight.

DJI Matrice 300 and LiDAR Livox MID 40

The DJI M300 Drone sensor is integrated with the LiDAR Livox MiD 40 and the camera via the payload. The payload system can carry a Livox MID 40 lidar sensor. Then a trial of the DJI M300 was carried out to bring the existing payload according to the CNC

design. LiDAR Livox MID 40 has an acquisition design to map the surrounding environment. Point Cloud provides detailed measurements in the form of a circular laser with a data acquisition center. Mid-40 equals a 32-line point cloud product when the integration time is 0.1 seconds. Data acquisition can provide an area sweep with a data frame range of 3000 m/s.

Figure 3. Payload Design on DJI M300 and LiDAR Livox

The Livox Mid-40 LiDAR sensor can detect objects as far as 260 meters. LiDAR uses a sophisticated circular scanning pattern to provide highly accurate details. The LiDAR MID 40 is already in mass production and ready for immediate delivery to facilitate use in autonomous driving, robotics, mapping, security, and other areas.

Result and Discussion

Table 1. Number of Volume Measurement Points

Total Station	IPAD LiDAR	Low-Cost Drone LiDAR
43 points	1048576 points	1170 points

The measurement of Salt Stockpile Volume is carried out by measuring three methods. The terrestrial method is carried out with a Total Station, and the UAV method is with a Low-Cost Drone. IPAD measurements were carried out as supporting data for the two methods that have been carried out. The measurement time for the total station method is 1-hour, Low-Cost Drone 15 minutes, and LiDAR IPAD 15 minutes. The most measurement points were obtained from LiDAR measurements of 1048576 points, and the lowest point was the terrestrial method with 43 points. This is because each method

has a different measurement capacity according to the needs of measuring the salt stockpile volume.

Based on the obtained visualization of the measurements carried out using the Total Station, IPAD, and Low-Cost Drone methods. The volume resulting from terrestrial measurements is 724.383044 cubic meters, with a validation value to be used as a reference for actual data. The red color represents GNSS acquisition data when measuring volume. At the same time, the light blue color is validation data using the Terrestrial measurement method using the Total Station tool. IPAD measurements are used as additional data in volume measurements.
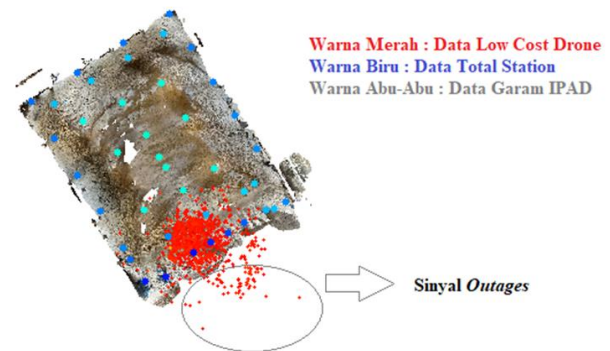
Figure 4. Overlapping of Volume Measurement Results

Table 2. Results of Volume Standard Deviation Analysis

Results of Volume Standard Deviation Analysis	IPAD LiDAR Standard Deviation	Standard Deviation of LiDAR Low-Cost Drones
Easting: 7.635	Easting: 2.667	Easting: 2.664
Northing: 8.734	Northing: 2.347	Northing: 2.247
Z: 1.6586	Z: 1.878	Z: 1.833

In table 2, a statistical test is carried out on the measurement volume. The standard deviation is used to determine each data distribution level. The data is used to perform filtering outages that occur in measurements. The distribution of the Low-Cost Drone data is to help with volume calculations. Based on LiDAR measurements, IPAD has a volume of

720.23167 cubic meters. At the same time, the lowest value is obtained from the measurement value of the Low-Cost Drone of 324,688 cubic meters. Low-Cost Drone measurements have the most significant difference due to signal outages during the data acquisition. LiDAR data retrieval is not comprehensive from the Stockpile form due to the narrow space between the Stockpile and the roof of the building.

Table 3. RMS Volume Measurement Error

RMS Error	RMS Error value	Difference Between Methods
Result of RMS Error between Total Station and IPAD	0.822496 meter	TS+IPAD – TS+Drone= -3.104
RMS Error Results between Total Stations and Low Cost Drones	3.92697 meter	TS+Drone-Drone+IPAD= 2.383
RMS Error Results between Low Cost Drones and IPAD	1.54346 meter	Drone+IPAD-TS+IPAD=0.7209

In table 3, to find out the RMS Error Validation value is done to check the accuracy between methods. The method used as a reference during the georeferencing process is the terrestrial method. Measurement of the RMS error results between the total station and IPAD has better results because the value is smaller than the other methods. These results are due to the volume of data acquisition between Total Station and IPAD does not have problems in the form of signal outages.

Georeferencing

Figure 5. Georeferencing

Georeferencing is a process of labelling coordinates in the form of positional calibration of raster data in the form of images. These coordinates are obtained from the measurement results of Salt Land as reference data. Livox MID 40 data which still has local coordinate

data from a measurement, becomes a global coordinate system. This method is used to integrate all local observation data into one coordinate system. Georeferencing uses the reference point of the Low-Cost GNSS measurement results. Geographical data needs to be aligned with the coordinates of the measurement results that have been carried out so that they can be exactly in the Satellite Image data.

In Figure 6. RMS Error 4.801 is generated, which is processed in the Cloud Compare application. The RMS error value, which has a small value, is said to be more accurate than the estimation method, which has a more significant Root Mean Square Error (RMSE). The RMS Error measurement is used to evaluate the results of data retrieval of the results of linear regression measurements of salt lands by measuring the accuracy of the estimates of a model.

Table 4. Comparison of Area of Salt Land Measurement Results

Parameter	GNSS Low Cost	LiDAR Livox MID 40
Salt Land 2400 Square meters	2550 Square Meters	2542 Square Meters

Measurement validation was carried out by calculating the area of 15 x 80 meters of salt land for one salt field. Salt field measurements produce Low-Cost GNSS data with manual calculations having a difference of 150 square meters. This is because the salt fields do not have a fixed land area because they are built in a semi-permanent form, so they are easily affected by the weather. The difference in the form of the Low-Cost GNSS with the LiDAR Livox MID 40 is quite significant due to the difference in reference between the two. LiDAR Livox MID 40 data have a local reference, and Low-Cost GNSS has a WGS 84 reference converted to UTM 49 S coordinates. In addition, the data objects detected by the LiDAR Livox MID 40 are only two salt fields. The measurement error data for salt land has a better correction value of 5.91%. Measurements with LiDAR Livox MiD-40 have a better level of accuracy because LiDAR data can map the topography in more detail. LiDAR has absolute and relative accuracy for better modelling and more realistic interpretation. This is used during acquisitions, such as calculating the height of objects and sorting out land boundaries and the surrounding water.

Figure 6. Georeferencing Position Figures
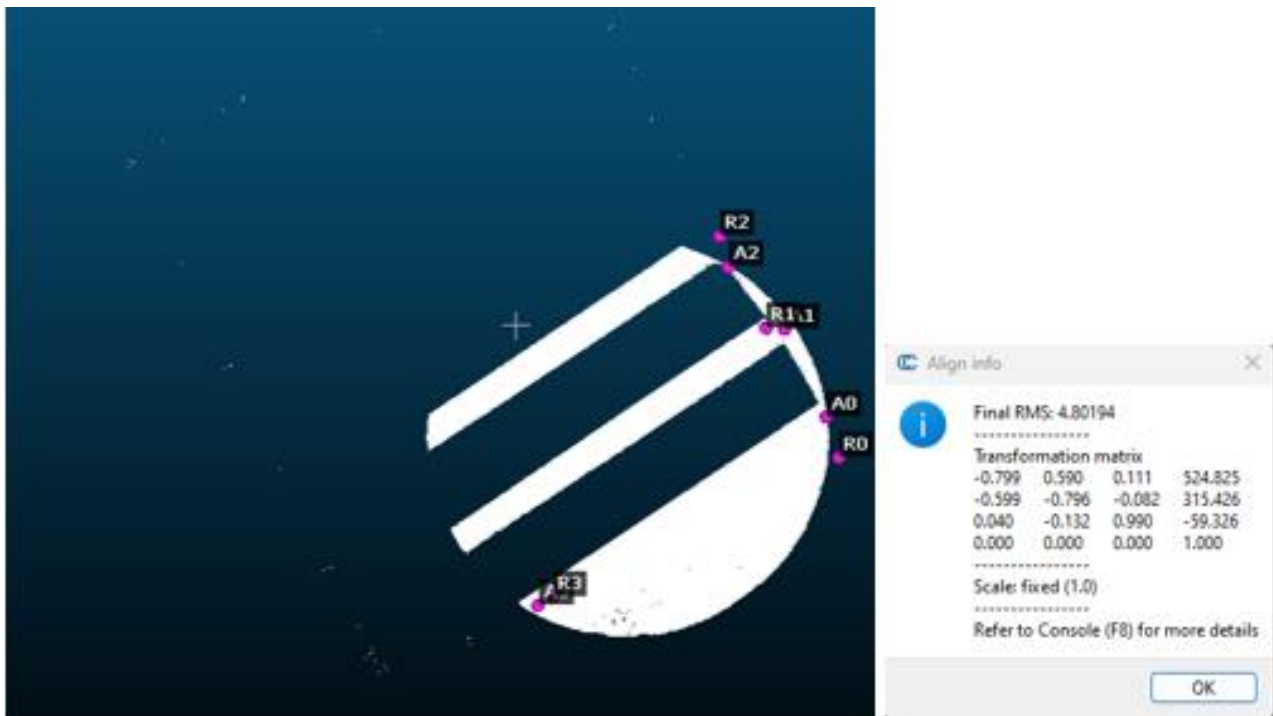
Figure 7. Comparison Results of Root Mean Square Error Total Station with LiDAR Livox MID 40

Table 5 shows the results of the area geometry accuracy test carried out based on a standard error percentage value of less than 2%. This calculation was carried out with a value of 5.91% for the LiDAR Livox MiD 40 accuracy test. This is because LiDAR Livox MID 40 measurements have better quality point cloud data than Low-Cost GNSS data.

Table 5. Standard Level of Measurement based on Land Area

Low Cost GNSS	LiDAR Livox MID 40
6.25 %	5.91 %

Table 6. Number of Salt Land Acquisition Result Points

Number of IPAD Points	Number of Low cost GNSS Points	Number of Livox MID 40 points
8139611 points	28 points	1974360 points

Conclusion

Researchers can conclude that making a three-dimensional visualization of PT. Salt for measurement efficiency has not been optimally carried out. Volume Low-Cost Drone has a small volume value due to the use of LiDAR, which can only process the coverage area of only one point cloud line. Besides that, drones are still unstable to fly statically to retrieve data optimally. The analysis process for modelling accuracy test results was carried out using three methods: height correction, area error correction, and volume correction. Volume Correction has a different value of 399,694 meters3 between the Total Station and the Low-Cost Drone. This is because there is poor data acquisition to produce salt stockpile areas. In addition, there are many signal outages because the measurements are carried out in the Warehouse. The measurement error data for salt land has a better correction value of 5.91%. Measurements with LiDAR Livox MiD-40 have a better level of accuracy because LiDAR data can map the topography in more detail. LiDAR has absolute and relative accuracy for better modelling and more realistic interpretation. This is used during acquisitions, such as calculating the height of objects and sorting out land boundaries and the surrounding water.
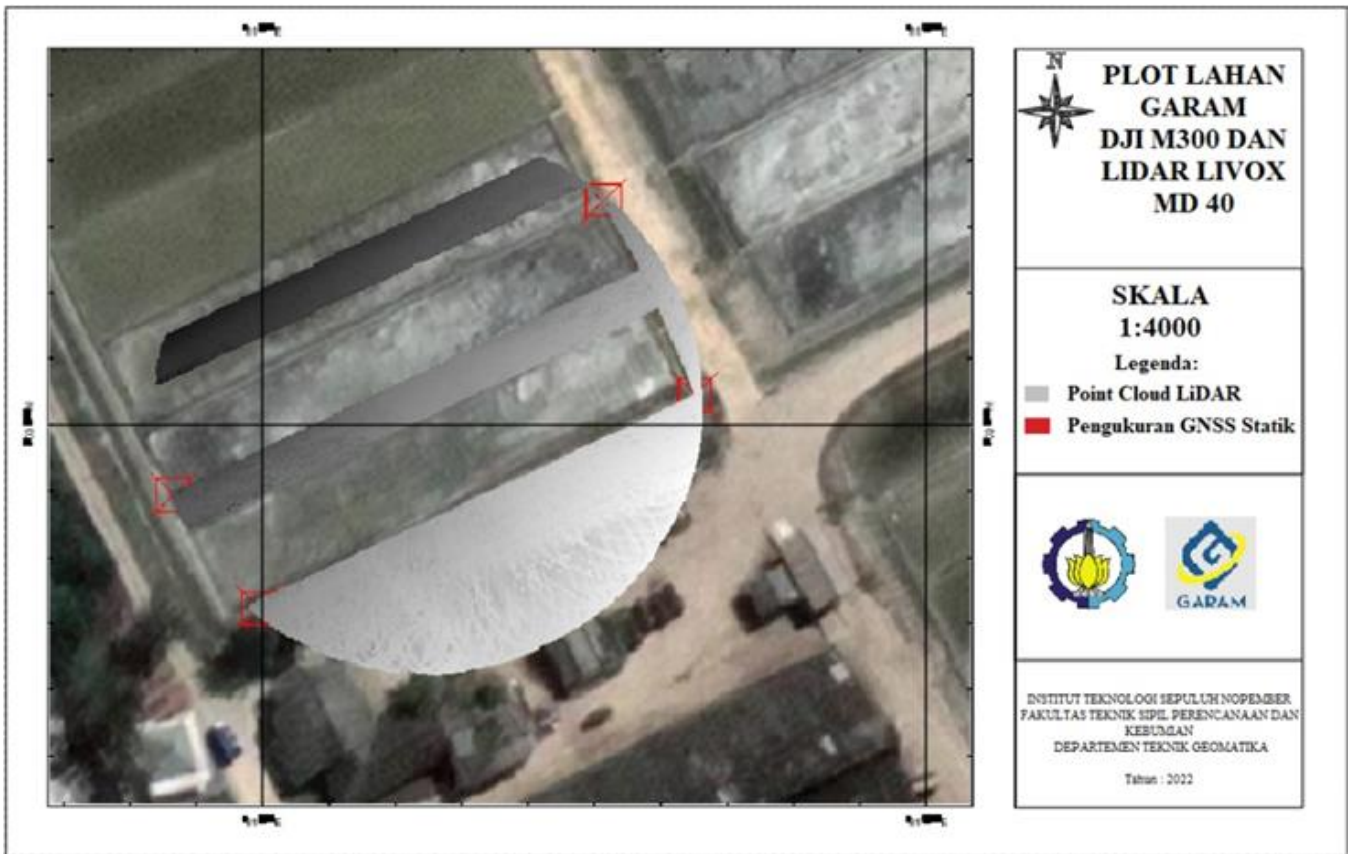
References

[1] Adamopoulos, E., Rinaudo, F. UAS-based archaeological remote sensing: Review, meta-analysis and state-of-the-art, *Drones*. **4(3)** (2020) 46.

[2] Barba, S. M. Accuracy assessment of 3D photogrammetric models from an unmanned aerial vehicle, *Drones*. **3(4)** (2019) 79.

[3] Bhowmik, Avit Kumar. Evaluation of Spatial Interpolation Techniques for Mapping Climate Variables with Low Sample Density. Disertasi. Portugal: University Novade Lisboa, 2012.

[4] Badan Standardisasi Nasional. Standar Nasional Indonesia Jaring kontrol horizontal, 2002.

[5] Cahyadi, Mokhammad Nur. Comparison analysis of accuracy and precision on GNSS K706 Oem Board and GPS Topcon HiperPro [Journal] // IOP Conference Series: Earth and Environmental Science. - [s.l.] : IOP Conference Series: Earth and Environmental Science, - Vol. 4th, 2019.

[6] Cahyadi, Mokhammad Nur. Comparative Analysis of Low-Cost GNSS OEM Board K706 AND BX316 [Journal] // IOP Conference Series: Earth and Environmental Science, 2020.

[7] Diego Ronchi, Marco Limongiello, and Salvatore Barba, Department of Civil Engineering, University of Salerno, 84084 Fisciano, Italy; diego.ronchi@spiron.it (D.R.); sbarba@unisa.it (S.B.) Spiron Heritage and Survey, 00198 Rome, Italy, 2020.

[8] Elbahnasawy Magdy et, al, Multi-Sensor Integration Onboard a UAV-Based Mobile Mapping System for Agricultural Management Lyles School of Civil Engineering, Purdue University, USA, 2018.

[9] Fernández Hernandez, J., González-Aguilera, D., Rodríguez-Gonzálvez, P., Mancera-Taboada, J. Image-based Modelling from unmanned aerial vehicle (UAV) photogrammetry: An e_ective, low-cost tool for archaeological applications, *Archaeometry*. **57** 128–145.

[10] Gao Yanbin. INS/GPS/LiDAR Integrated Navigation System for Urban and Indoor Environments Using Hybrid Scan Matching Algorithm [Book], 2015. Available from: www.MIDpi.com/journal/sensors

[11] Ghilani, C. D., & Wolf, P. R. Elementary Surveying an Introduction to Geomatics. New Jersey: Pearson Education Inc, 2015.

[12] Groves, P.D. Principles of GNSS, Inertial, and Multisensor Integrated Navigation Systems. Boston: Artech House, 2008

[13] Hidayat. 3D Feature Positioning in Historical Building Using Spherical Panoramic Image Mosaics: Case Study Surabaya City Hall Front

Façade. 34th Asian Conference on Remote Sensing, 2013 1 (1), 4674.

[14] Jose, J. M. Performance comparison of Extended and Unscented Kalman Filter implementation in INS-GPS integration. Prague: Lulca University of Technology, 2009.

[15] Lasse Klingbeil. Towards Autonomous Navigation of an UAV-based Mobile Mapping System. International Conference on Machine Control & Guidance. Institute of Geodesy and Geoinformation, University of Bonn, 2014.

[16] Malberg, J,A. Salt Stockpile Inventory Management Using LiDAR Volumetric Measurements. Remote Sensing. MIDPI 14, 4802, 2022.

[17] Mardiyanto, Ronny. Robot Operating System (ROS) Framework for swarn Drone Flight Controller. International Seminar on Intellegent Technology and Its Application. IEEE Xplore 978-1-6654-6081-1/22/$31.00, 2022.

[18] Michael, Edward and Gordon Gracie. (1981). Analysis Adjustmentof Survey Measurement. New York: Van Nostrand Reinhold Company.

[19] Rafatnia, S. and Mirzaei, M. Estimation of reliable vehicle dynamic model using IMU/GNSS data fusion for stability controller design. Mechanical Systems and Signal Processing, 168 (2022) p.108593.

[20] S. Scheller, P. Westfeld a, D. Ebersbach. Calibration of a Mobile Mapping Camera System with Photogrammetric Methods. Institute of Photogrammetry and Remote Sensing, Technische Universität Dresden, 01062 Dresden, Germany, 2007.

[21] Spesifikasi Teknis Peraturan Menteri Negara Agraria (PMNA), Kepala Badan Pertanahan Nasional (BPN) Nomor 3 Tahun 1997 Tentang Toleransi Persentase Beda Luas Tanah.

[22] Shao Zhenfeng. Spatio-temporal-spectral-angular observation model that integrates observations from UAV and mobile mapping vehicle for better urban mapping. Geo-spatial Information Science. State Key Laboratory of Information Engineering in Surveying, Mapping and Remote Sensing, Wuhan University, Wuhan, China, 2021.

[23] Stoter, J.E. 3D Cadastre. Delft: Departement of Geodesy, Faculty of Civil Engineering & Geosciences, Technical University Delft, 2004

[24] Taufik, Muhammad. Analysis level of accuracy GNSS observation [Journal] // IOP Conference Series: Earth and Environmental Science. - [s.l.] : IOP Conference Series: Earth and Environmental Science, - Vol. 4th, 2019.

[25] Tan, S. Concept of Satellite Navigation and the Principle of Positioning and Velocity Measurement. in GNSS Systems and Engineering: The Chinese Beidou Navigation and Position Location Satellite, Wiley, 2018, pp.117-132.

[26] Yuwono, (). Assessment of the Single Frequency Low Cost GPS RTK [Journal]. - Indonesia : IOP Conference Series: Earth and Environmental Science, - Vol. 4th, 2019

[27] Z. C. He. An edge-based smoothed tetrahedron finite element method (ES-T-FEM) for 3D static and dynamic problems. Comput Mech: 52, 2013 221–236.

IDENTIFICATION OF GROUNDWATER POTENTIAL USING GEOGRAPHIC INFORMATION SYSTEMS AND REMOTE SENSING (CASE STUDY: MOJOKERTO REGENCY)

Beata Alpha Christina Sulle[1] Dedy Kurnia Sunaryo[1], Adkha Yulianandha[1]

[1] School of Geodesy, Malang National Institute of Technology, Malang, Indonesia
E-mail: beatachristina28@gmail.com

ABSTRACT

The impact of the drought problem in Mojokerto Regency resulted in thousands of people having access to clean water. So, it is necessary to plan the utilization of groundwater resources well. Therefore, more serious handling is needed in an effort to overcome the problem of groundwater supply. One of them is the availability of groundwater potential maps. This study aims to determine the identification of aquifer potential and groundwater potential in Mojokerto Regen cy in 2020. This research uses SPO T - 7 satellite imagery to see vegetation density using the NDVI method and uses 5 parameters, namely rainfall, soil texture, rock type/geology, slope, and land use. This study used the AHP method in determining the priority weight value of each parameter. Based on the results of the study, the results were obtained with 3 classifications with the largest area being an area with mode rate groundwater potential of 52,621.285 Ha and the smallest area being an area with low groundwater potential of 2,426.327 Ha. Previous research identified groundwater potential using the NDVI method with Landsat 8 imagery which has a resolution of 30 meters. Therefore, this research is expected to produce better vegetation density by using SPOT-7 imagery to obtain more detailed groundwater potential, because the resolution of the image SPO T -7 is 6 meters. So that this research can be considered in efforts to process the potential of groundwater resources in Mojokerto Regency.

Keyword: Groundwater Potential, Aquifer, AHP, SPOT-7, NDVI.

Introduction

Groundwater is rainwater runoff that flows beneath the earth's surface and forms geological stratification, potential differences in soil moisture, and gravitational forces. Surface water is often referred to as groundwater (Asdak. 2010). In areas that often experience drought, resulting in difficulties with clean water. Mojokert o Regency is one of the areas that is classified as drought-pro ne (Kusuma. 2018). To deal with the proble m of drought, it is necessary to deal with the supply of clean water by providing a map of groundwater potential. Identification of groundwater potential in previous research is by utilizing geospatial information system metho ds and remote sensing metho ds. In previous studies, potential areas of groundwater have been identified with a geographic information system used to obtain aquifer maps using a tiered quantitative overlay method on several parameters.

The parameters used to obtain the distribution of potential aquifers are vegetation density, slope, soil texture, rainfall and land use. From the overlay results obtained, an overlapping process will be carried out between the distribution of the aquifer potential and the groundwater basin parameters to obtain the distribution of groundwater potential. Remote sensing is used to provide information on vegetation density generated by the NDVI (Normalized Difference Vegetation Index) method. From previous research the ND VI (Normalized Difference Vegetation Index) method with Landsat 8 imagery has a resolution of 30 meters. To get better results of vegetation density, identify the NDVI Algorithm (Normalized Difference Vegetation Index) using SPOT-7 Imagery with a resolution of 6 meters. The Analytica l Hierarchy Process (AHP) is a Geographic Information System

(GIS) calculation metho d that can be used as an approach to assessing groundwater potential. The AHP methodology facilitates objective decision-making.

It is hoped that this research can provide information in identifying aquifer potential and groundwater potential based on Geographic Information Systems and Remote Sensing in Mojokerto Regency. Which later can be used as information material in dealing with drought and scarcity of groundwater.

Methodology

In identifying areas that have the potential to have groundwater in the Mojokerto Reg enc y area, namely by using the Geographic Information System and Remote Sensing methods. Where the Geographic Information System is used to obtain aquifer maps using a tiered quantitative overlay method on several parameters. The parameters used to obtain the distribution of potential aquifers are vegetation density, slope, soil texture, rainfall and land use. From the overlay results obtained, an overlapping process will be carried out between the distribution of the aquifer potential and the groundwater basin parameters to obtain the distribution of groundwater potential. Remote sensing is used to provide information regarding vegetation density generated by the NDVI method from SPOT -7 imagery.

Vegetation Index

Vegetation index is a form of spectral transformation that is applied to multi-channel images to highlight aspects of vegetation density or other aspects related to density, for example biomass, Leaf Area Index (LAI), chlorophyll concentration, and so on. Practically, this vegetation index is a mathematical transformation that involves several channels at once, and produces new, more representative images in presenting vegetation phenomena (Arnanto, 2013). Vegetation index or NDVI is an index that describes a plant based on the level of greenness. The vegetation index is a mathematical combination between the red band and the NIR (Near-Infra red Radiation) band which has long been used as an indicator of the presence and condition of vegetation (Lillesand and Kiefer, 1979).

$$\text{NDVI} = \frac{(NIR - RED)}{NIR + RED} \tag{1}$$

Table 1. Vegetation Density Index Class

Range of Vegetation Index Values	Score	Influence Level
0,36 – 1	4	Influential
0,26 – 0,35	3	Currently
0,15 – 0,25	2	Less Influence
(-0,03) – 0,15	1	Very Less Influenced
(-1,0) – (-0,03)	5	Very influential

Accuracy Tests

Accuracy tests performed on this category of data in general are tests of visual interpretation results, digital classification, and grouping of values resulting from spectral transformation. The technique used is a contingency table which in remote sensing is better known as a confusion matrix table. The confusion matrix table is a matrix table that connects the pixels resulting from the classification and ground truth data whose information can be retrieve d from verified field data and maps. There is a lot of information that can be retrieved from the confusion matrix, including overall accuracy, producer accuracy, user accuracy, kappa coefficient, and tau coefficient (Wicaksono, 2010). Field validation is done by making a confusion matrix to get the overall accuracy value. The overall accuracy value shows the number of pixels that are classified correctly in each class compared to the number of samples used to test accuracy in all classes, using the following formula (Wicaksono, 2010):

$$\text{Overall accuracy (\%)} = \frac{\text{the number of pixels that are correctly classified}}{\text{number of accuracy test samples}} \times 100 \tag{2}$$

Analytical Hierarchy Process (AHP)

The Analytical Hierarchy Process (AHP) method is a decision support method developed in 1980 by Thomas L., Saaty. In this method the existing problems are described in hierarchical form, the hierarchy created consists of several levels starting with objectives, criteria, and alternatives. The steps in performing calculations on the AHP method consist of three levels: the purpose of the decision is at the top level, followed by the second level consisting of criteria then the alternatives are at the third level for evaluation.

Classification of Groundwater Potential

Classification is carried out to determine the level of groundwater potential for area development, and the

groundwater supply capability of each level (Sholicin, Asmaranto and Jannati, 2014).

Then to determine the level of suitability as a water catchment area is done by adding up the multiplication results between the weight values and scores in each parameter class, using the formula:

$$\text{Nilai Total} = (Nb*Np) + (Bb*Bp) + (Cb*Cp) + (Tb*Tp) + (Kb*Kp) + (Lb*Lp) \quad (3)$$

Making class intervals uses the following formula (Sigit. 2011):

$$i = \frac{Kt - Kr}{k} \qquad (4)$$

Result and Discussion

Identify areas that have the potential to have groundwater in the Mojokerto Regency area, namely by using the Geographic Information System and Remote Sensing methods. Where the Geographic Information System is used to obtain aquifer maps using a tiered quantitative overlay method on several parameters. The parameters used to obtain the potential distribution of aquifers are vegetation density, slope, soil texture, rainfall and land use. From the overlay results obtained, an overlapping process will be carried out between the distribution of the aquifer potential and the groundwater basin parameters to obtain the distribution of groundwater potential.

Remote sensing is used to provide information regarding vegetation density generated by the NDVI method from SPOT-7 imagery.
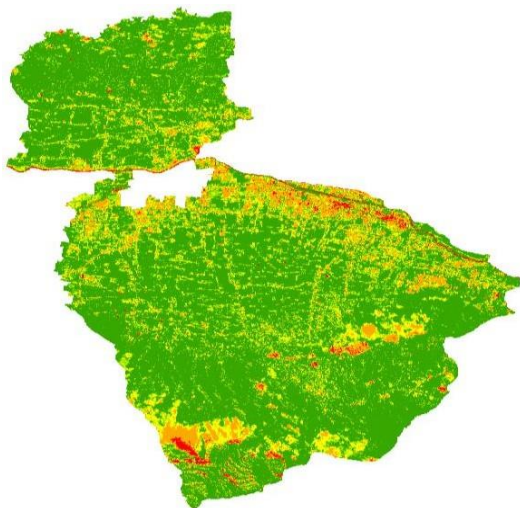
Vegetation Index Data

Figure 1. Results of vegetation index data with NDVI (Normalized Difference Vegetation Index) algorithm processing

The results of vegetation data using the NDVI algorithm calculation is an index that describes a plant based on its greenness level.

Confusion Matrix Accuracy Test

The results are then used as an accuracy test material to obtain the confidence level value of the classification results on images with density measurement data from field surveys as a reference for calculating the confusion matrix (accuracy test matrix). The following is the result of the confusion matrix calculation in this study as shown in table 2.

Table 2. Confusion Matrix Accuracy Test

Image Classification	Field Survey				Correct Amount	Number of Rows
	Very influential	Very Less Influenced	Less Influence	Currently	Influential	
Very influential	18	0	0	0	0	18
Very Less Influenced	0	18	0	0	0	18
Less Influence	0	0	16	2	0	18
Currently	0	0	1	17	0	18
Influential	0	0	0	1	17	18
Correct Amount					86	
Number of Columns	18	18	17	20	17	90

rom the confusion matrix table above, the total accuracy calculation is then performed as follows:

$$\text{Overall accuracy (\%)} = \frac{\text{the number of pixels that are correctly classified}}{\text{number of accuracy test samples}} \times 100 \qquad (5)$$

$$= \frac{86}{90} \times 100 \qquad (6)$$

$$= 95.56\% \qquad (7)$$

AHP Processing Results

From the process of determining the weight of aquifer potential and groundwater potential using six parameters in the calculation; Vegetation Density(NDVI) is a param e t er to identify aquifer potential areas and groundwater potential from the proximity of vegetation density factors, land use is a parameter to identify potential aquifer areas and groundwater potential from the type of land use of origin, rainfall is a parameter to identify potential aquifer areas and groundwater potential from the annual rainfall factor, slope is a parameter to identify aquifer potential areas and groundwater potential from the topographic slope factor, soil texture is a parameter to identify potential aquifer areas and groundwater potential from the soil texture of origin, rock type is a param e t

er to identify aquifer potential areas and ground water potential from the type of rock of origin.

Table 3. Criteria Weighting Matrix Results

Criteria	Total Weight
NDVI	7.04%
land use	15.03%
rainfall	24.42%
slope	17.86%
soil texture	5.55%
rock type	30.11%
Total	**100.00%**

From the calculation results above it is known that the order of priority for each parameter is as follows:

1. Rock Type Criteria has the first highest weight, namely 30.11%
2. The Rainfall Criterion has the second highest weight, namely 24.42%
3. The slope criterion has the third highest weight, namely 17.86%
4. Criteria for Land Use has the fourth weight, namely 15.03%
5. The Vegetation Density Criterion has the fifth weight, namely 7.04%
6. Soil Texture Criteria has the sixth weight, namely 5.55%

Thus, class parameter weighting for aquifer potential and groundwater potential.

Parameter Data Processing

The aquifer potential identification map is obtained from the process of scoring and weighting then overlaid between vegetation, rock type, rainfall, slope, soil type, land use, and groundwater basin. Then choose between the parameters to be overlaid in stages between the two parameters in one overlay process, with the first overlay stage namely Vegetation Index with Rock Graduation, then from the overlay results go to the second overlay process with Soil Texture, followed by the third overlay process with Slope, then the fourth overlay with Rainfall and the last overlay with land use. Then add up the loyal scores of overlapping parameters, the results of which will be classified into the aquifer potential class with the class values as follows:

$$KI = \frac{105-63}{3} = 14 \qquad (8)$$

3 classes are used with score intervals, the results of which can be seen in the following figure 2.

Table 4. Aquifer potential classification

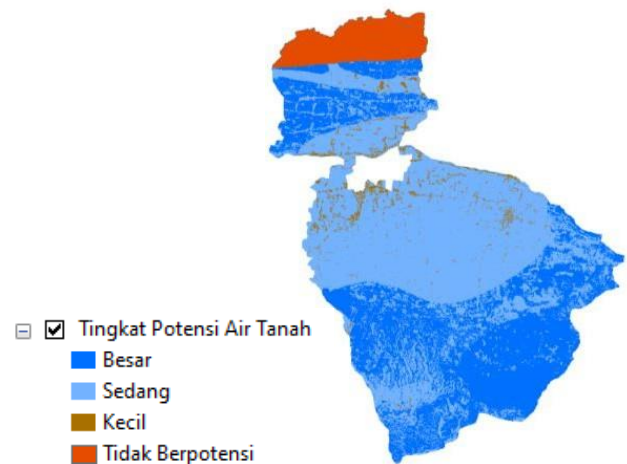| Class Intervals	Aquifer Potential Class
91 - 105	Big
77 - 90	Currently
63 - 76	Small

Figure 2. the results of the calculation of the Analytical Hierarchy Process (AHP) and classification into groundwater potential data.

Groundwater Potential Validation Test

From the results of observing the distribution of drilled wells from each class of groundwater potential, the amount of spring water discharge is obtained with discharge values as follows: Large (> 50 litters/ second), Medium (25-50 litters/ second), and Small (<25 litters /second). The distribution of drilled wells can be seen in the following figure:
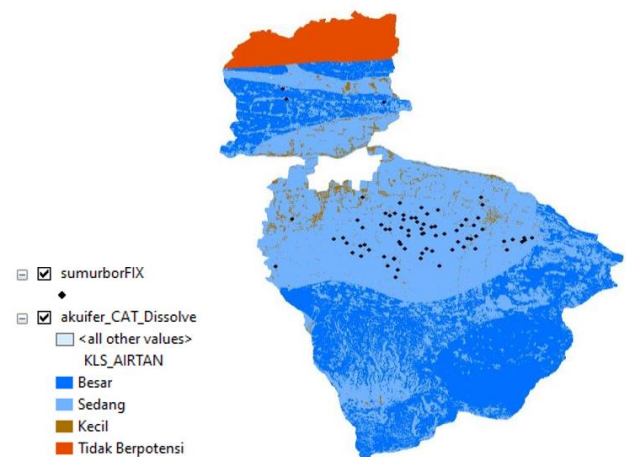

Figure 3. results of groundwater potential data and data on the distribution of drilled well points.

Table 5. Test the accuracy of the potential groundwater confusion matrix

Groundwater Potential Map	Borehole Discharge Point			Correct Amount	Amount Line
	No Potential	Small	Medium	Big	
No Potential	0	0	0	0	0
Potential	0	45	0	1	46
Small	0	8	20	0	28
Medium	0	2	0	2	4
Big				11	
Total	0	55	20	3	78

From the confusion matrix table above, the total accuracy calculatio n is then carried out as follows (Wicak so no , 2010):

$$\text{verall accuracy (\%)} = \frac{\text{the number of pixels that are correctly classified}}{\text{number of accuracy test samples}} \times 100 \qquad (8)$$

$$= \frac{67}{78} \times 100 \qquad (9)$$

$$= 85,89\% \qquad (10)$$

Conclusion

In utilizing the SPOT-7 Geographic Information and Imagery System in identifying groundwater potential with a case study in Mojokerto Regency, the results of groundwater potential areas in Mojokerto Regency show that the largest area is an area with moderate groundwater potential of 52,621.285 Ha and the smallest area is an area with low groundwater potential of 2,426.327 Ha and the results of the groundwater potential validation use the borehole discharge point with a conformity percentage of 85.89%. Of the 90 data obtained 73 appropriate data and 17 inappropriate data.

References

[1] Abdelhamid, Ramadan, and Z. Eldin, A decision support system for performance evaluation, IJCA Special Issue on Computational Intelligence & Information Security CIIS 2012, 2012, pp. 1-8.

[2] Afshari, A., Mojahed, M. and Yusuff, R.M, Simple additive weighting approach to personnel selection problem, *International Journal of Innovation, Management and Technology*. **1(5)** (2010) 511.

[3] Agarwal, R., & Garg, P. K., Remote Sensing and GIS Based Groundwater Potential & Recharge Zones Mapping Using Multi-Criteria Decision-Making Technique, *Water Resources Management*. **30(1)** (2016) 243–260. DOI :10.1007/s11269-015-1159-8

[4] Amanu. Kekeringan di Mojokerto Meluas, Jadi 8 Desa, 2018 [Online]. Available from: https://faktualnews.co/2018/10/04/kekeringan-di-mojokerto- meluas-jadi-8-desa/102264/ [diakses 14 Oktober 2021]

[5] Aristiwijaya, Bayu, Identification of Potential Water Sources Using Langsat 8 Satellite Imagery and Geographic Information Systems (Case Study: Bojonegoro Regency). Surabaya: FTSP-ITS Geomatics Engineering Study Program, 2015

[6] Arnanto, Ardi, Utilization of Normalized Difference Vegetation Index (NDVI) Transformation of Landsat Tm Imagery for Vegetation Zoning on the Southern Slopes of Merapi. Yogyakarta: National Land College.

[7] Benítez, J., Delgado-Galván, X., Gutiérrez, J.A. and Izquierdo, J, Balancing consistency and expert judgment in AHP, *Mathematical and Computer Modelling*. **54(7)** (2011) 1785- 1790.

[8] Budianto, Enggran Eko Budiant, Five Villages in Mojokerto Subscribe to Clean Water Drought During the Dry Season, 2019 [Online]. Available from: https://news.detik.com/berita-jawa-timur/d-4598848/lima-desa-di-mojokerto-langganan-krisis-air-bersih-saat-musim-kemarau

[9] Danoedoro P, Digital Image Processing Theory and Its Application in the Field of Remote Sensing. Faculty of Geography, Gadjah Mada University, 1996.

[10] Danoedoro P, Digital Image Processing: Theory and Its Applications in the Field of Remote Sensing. Yogyakarta: Gadjah Mada University, 2014

[11] ESA, Sentinel-2 User Handbook, ESA Standard Document User Handbook, European Space Agency, 2015

[12] Fadlillah, Mochammad Fajar, Rintis Hadiani dan Solichin, Hydrological Drought Analysis Based on the Normalized Difference Vegetation Index (NDVI) Method in the Alang River Basin, Wonogiri Regency. Surakarta: Eleven March University.

[13] Herlambang, A., Kualitas Airtanah Dangkal di Kabupaten Bekasi, Tesis: Istitut Pertanian Bogor, 1996.

[14] Kittur, J., June, Optimal generation evaluation using SAW, WP, AHP and PROM ETHEE multi-Criteria decision making techniques. In Advancements in Power and Energy (TAP Energy), 2015 International Conference on (pp. 304-309). IEEE.

[15] Kodoatie, Robert J., Tata Ruang Air Tanah. Penerbit Andi, Yogyakarta, 2012.

[16] Kusuma, Wahyu Widya dan Adjie Pamungkas, Directions for Drought Hazard Adaptation in Mojokerto Regency. Surabaya: Ten November Institute of Technology, 2018.

[17] Lillesand, T.M., and R.W. Kiefer, Remote Sensing and Image Interpretation. Translated by: Dulbahri. Yogyakarta: Gajah Mada University Press, 1994.

[18] Lintang, Nuansa Chandra, TjaturahonoBudi Sanjoto dan Heri Tjahjono, Kajian Kerapatan

[19] Vegetasi Hutan Lindung Gunung Ungaran Jawa Tengah Tahun 2016 Menggunakan Metode Indeks Vegetasi. Semarang: Universitas Negeri Semarang, 2016.

[20] Mather, P.M.. Computer Processing of Remotly Sensed Data. Jhon Willey& Sons, London, 1987

[21] Norhadini, Karina, Musim Kemarau, Delapan Kecamatan di Mojoketro Alami Kekeringan, 2020. [Online] Available from: https://jatimnet.com/musim-kemarau-delapan-kecamatan-di-mojokerto-alami-kekeringan

[22] Nurmalasari, Intansania dan Santosa, Sigit Heru Murti Budi, Pemanfaatan Citra Sentinel- 2A untuk Estimasi Produksi Pucuk Teh di Sebagian Kabupaten Karanganyar. Yogyakarta: Univesitas Gadjah Mada, 2016.

[23] Pemerintahan Kabupaten Mojokerto, Geografis. [Online] Available from: https://id.wikipedia.org/wiki/Kabupaten_Mojok erto

[24] Prabowo, N. W., V. P. Siregar, and S. B. Agus. Klasifikasi habitat bentik berbasis objek dengan algoritma support vector machines dan decision tree menggunakan citra multispektral spot-7 di Pulau Harapan dan Pulau Kelapa, *Jurnal Ilmu dan Teknologi Kelautan Tropis.* **10(1)** (2018) 123-134

[25] Prahasta Eddy, Konsep – Konsep Dasar Sistem Informasi Geografi, Informatika, Bandung, 2001.

[26] Pratama, Adi Ifan, Abdi Sukmono dan Hana Sugiastu Firdaus, Identifikasi Potensi Air Tanah Berbasis Penginderaan Jauh dan Sistem Informasi Geografis, Semarang: Universitas Diponegoro, 2018.

[27] Prihatini Misti, 6 Desa di Kabupaten Mojokerto Dilanda Kekeringan, 2019. [Online] Available from: https://beritajatim.com/peristiwa/6-desa-di-kabupaten-mojokerto- dilanda-kekeringan/

[28] Putra Andi Rachman, Analisa Potensi Air Tanah Pada Cekungan Air Tanah Brantas, Surabaya: Institut Teknologi Sepuluh Nopember, 2018.

[29] Putri Dini Ramanda, Abdi Sukmono dan Bambang Sudarsono, Analisis Kombinasi Citra Sentinel-1a Dan Citra Sentinel-2a Untuk Klasifikasi Tutupan Lahan, Semarang: Universitas Diponegoro, 2018

[30] Razandi, Y., Pourghasemi, H. R., Neisani, N. S., & Rahmati, O., Application of analytical hierarchy process, frequency ratio, and certainty factor models for groundwater potential mapping using GIS, *Earth Science Informatics.* **8(4)** (2015) 867– 883. DOI: 10.1007/s12145-015- 0220-8

[31] Saaty, T.L., Vargas, L.G., Models, Methods, Concepts & Applications of The Analytic Hierarchy Process, Second Edition, Springer, New York, 2012

[32] Sholicin M., Asmaranto, Runi dan Jannati, Idelia, Analisa Satuan Kemapuan Lahan Kesediaan Air Tanah Kabupaten Pasuruan, Malang: Program Studi Teknik Pengairan Universitas Brawijaya, 2014

[33] Sigit, Agus Anggoro. Priyono dan Andriyani, Applikasi Sistem Informasi Geografis (Sig) Berbasis Web Untuk Monitoring Banjir Di Wilayah DAS Bengawan Solo Hulu, Surakarta: Universitas Muhammadiyah Surakarta, 2011.

[34] Sutanto, 1986. Penginderaan Jauh Jilid I. Yogyakarta: Gadjah Mada University Press. Susanto, 1994. Penginderaan Jauh Jilid II. Yogyakarta: Gadjah Mada University Press. Talobre D.F. 1967. La Mécanique des Roches.Deuxieme Edition. Dunod. Paris.

[35] Ulaf Kurnia dkk, Analisa Pola Spektral Citra Sentinel-2 (Spectral Analysis of Sentinel-2 Images), Jakarta Timur: Pusat Teknologi dan Data Penginderaan Jauh, Lembaga Penerbangan dan Antariksa Nasional, 2019.

[36] UU No. 07 Tahun 2004 Tentang Sumber Daya Air

[37] Yuhandri, Perbandingan Metode Cropping Pada Sebuah Citra Untuk Pengambilan Motif Tertentu Pada Kain Songket Sumatera Barat, Padang: Universitas Putra Indonesia YPTK, 2019